

**ARSENIC IMPAIRS EMBRYONIC LUNG DEVELOPMENT BY
MODULATING AIRWAY SMOOTH MUSCLE CONTRACTION VIA THE
CALCIUM/ CALMODULIN PATHWAY**

by

Christine Hillman

A thesis submitted to the Faculty of the University of Delaware in partial fulfillment of the requirements for the degree of Master of Science in Biological Sciences

Spring 2020

© 2020 Christine Hillman
All Rights Reserved

**ARSENIC IMPAIRS EMBRYONIC LUNG DEVELOPMENT BY
MODULATING AIRWAY SMOOTH MUSCLE CONTRACTIONS VIA THE
CALCIUM/CALMODULIN PATHWAY**

by

Christine Hillman

Approved: _____
Jason P. Gleghorn, Ph.D.
Professor in charge of thesis on behalf of the Advisory Committee

Approved: _____
Veila Fowler, Ph.D.
Chair of the Department of Biological Sciences

Approved: _____
John A. Pelesko, Ph.D.
Dean of the College of Arts and Sciences

Approved: _____
Douglas J. Doren, Ph.D.
Interim Vice Provost for Graduate and Professional Education and
Dean of the Graduate College

ACKNOWLEDGMENTS

I dedicate this thesis to the many people in my life to whom I am most gracious for. Thank you to Dr. Jason Gleghorn and the members of the Gleghorn lab. I would like to thank you to Rachel Gilbert and Brielle Hayward-Piatkovskiy for their patience and guidance as I completed my thesis.

Thank you to Dr. Brian Masters, Dr. Matthew Hemm, and Dr. Michelle Snyder of Towson University for reigniting my passion for the sciences and inspiring the curiosity that would lead to my decision to pursue this degree.

Thank you to everyone in my nursing family. Thank you to my nursing peers and mentors, and thank you especially to my patients, for providing me with the knowledge of how this education can be applied to help such amazing people.

Thank you to my friends and family. Thank you to my amazing sisters who I love so much and to my parents who have always believed in me. Thank you to Michael for your unwavering support and encouragement.

TABLE OF CONTENTS

LIST OF TABLES	vi
LIST OF FIGURES	vii
ABSTRACT	viii

Chapter

1	INTRODUCTION	1
	Arsenic, a Historical Perspective.....	1
	Arsenic is Everywhere.....	3
	Arsenic and Pathology.....	5
	Lung Development	12
	Airway Smooth Muscle and Its Role in Development.....	18
	Regulation of Airway Smooth Muscle Contraction	21
	Calcium/Calmodulin-Mediated Contractile Regulation Pathway	24
2	MATERIALS AND METHODS	28
	Overall Study Design	28
	CD1 Mouse and GCaMP Transgenic Mouse	29
	Ex Vivo Lung Culture	32
	Lung Structure Analysis (Immunofluorescence).....	35
	Western Blot.....	37
	Contraction Analysis and Kymograph Construction.....	40
	Calcium/Calmodulin Signaling Analysis	41
3	RESULTS.....	42
	Arsenic Affects Embryonic Lung Architecture.....	43
	Arsenic Affects Terminal Buds of Embryonic Lungs.....	44
	Arsenic Exposure Reduces the Frequency of Airway Smooth Muscle Contraction	46
	Smooth Muscle Quantification Studies	47
	Smooth Muscle Thickness Along Inner Bronchi	47
	Western Blot Quantification of α -Smooth Muscle Actin.....	48
	Arsenic Affects Calcium/ Calmodulin Signaling in Embryonic Lungs	49
4	DISCUSSION.....	51

Arsenic Exposure Increases the Risk of Respiratory Complications Associated with Preterm Labor	51
Arsenic Reduces the Number of Alveoli Precursors in the Lung, Increasing the Risk for Respiratory Pathologies	52
The Reduction in the Frequency of Airway Smooth Muscle Contractions Correlates with Underdevelopment of Arsenic-Exposed Lungs	54
Quantification of ASM by α -Smooth Muscle Actin Immunofluorescence is Limited and is Improved with Western Blot	55
Defective Calcium-Influx is the Underlying Mechanism of Arsenic- Exposed Lung Underdevelopment	56
5 CONCLUSION AND FUTURE WORK	59
Conclusion	59
Future Directions	60
REFERENCES	63
Appendix	
A CUSTOM MATLAB CODE	73
B IACUC Permission	77

LIST OF TABLES

Table 1.1:	Complications of Arsenic Exposure (Acute vs Chronic).....	6
Table 2.1:	Stages of Lung Development (Human vs Mouse).....	15

LIST OF FIGURES

Figure 1:	Global Distribution of the Probability of Arsenic Ground Water Contamination.....	4
Figure 2:	Proposed Mechanisms for Common Arsenic-Induced Pathologies.....	11
Figure 3:	Architecture of the Developing Embryonic Mouse Lung.....	13
Figure 4:	Branching Morphogenesis of the Developing Embryonic Mouse Lung.....	17
Figure 5:	Brightfield Image of Whole Lung Explant.....	18
Figure 6:	Smooth Muscle Contraction	23
Figure 7:	Regulation of Airway Smooth Muscle Contraction.....	26
Figure 8:	Dissection of E12.5 Mouse Lung.....	33
Figure 9:	Schematic of E13 Mouse Lung Culture.....	35
Figure 10:	Effect of Arsenic on Embryonic Lung Architecture.....	43
Figure 11:	Effect of Arsenic on Terminal Buds of the Embryonic Lung.....	44
Figure 12:	Kymograph Construction and the Effect of Arsenic on Airway Smooth Muscle Contraction Frequency in the Embryonic Mouse Lung.....	46
Figure 13:	Effect of Arsenic on Airway Smooth Muscle Thickness Along Inner Bronchi of the Embryonic Mouse Lung.....	47
Figure 14:	Effect of Arsenic on α -Smooth Muscle Actin Abundance in the Embryonic Mouse Lung.....	48
Figure 15:	Effect of Arsenic on Calcium/Calmodulin Signaling Events in the Embryonic Mouse Lung and Corresponding Contraction Analysis....	49

ABSTRACT

Millions of people world-wide are exposed to arsenic through contaminated water that is either consumed directly or through contaminated crops (Hughes et al., 2011).

Arsenic is a naturally occurring compound that is distributed all over the world and is associated with pathologies including malignancies of nearly all body organs, cardiovascular diseases, respiratory diseases, and preterm labor with varied symptom severity depending on the source and duration of exposure (Hasan et al., 2019, Wai et al., 2017). While mechanisms have been proposed for certain pathologies including cancer, and heart disease, the mechanisms underlying arsenic-induced respiratory pathologies and poor birth outcomes are not well characterized (Ratnaike, 2003, Singh et al., 2011). The majority of arsenic toxicology research studies adulthood exposure despite the knowledge that the developing fetus is exposed to arsenic through trans placental transport when a pregnant mother is exposed to arsenic (Gerber et al., 1982). There is a gap in knowledge regarding the mechanism in which arsenic contributes to respiratory diseases, especially in regards to in utero exposure to the developing fetus (Wai et al., 2017). This research examines if arsenic affects embryonic lung development by modulating airway smooth muscle (ASM) contractions via the calcium/calmodulin contractile pathway. This pathway has been implicated in arsenic-induced pathologies of other smooth muscles such as cardiac smooth muscle and vascular smooth muscle making it a logical pathway to consider when studying respiratory pathologies with associated ASM components (Singh et al., 2011).

Embryonic mouse lungs were cultured in presence and absence of arsenic and the phenotypes were assessed. This research revealed that arsenic-exposed lungs are underdeveloped in that they exhibit narrowing of the major airways of the lung in addition to fewer alveoli precursors (terminal buds). In addition, contractions of the ASM were visualized using timelapse bright field imaging which showed that arsenic-exposed lungs contract less frequently. Finally, a transgenic mouse line was used to study the calcium/calmodulin mediated contraction pathway. These mice autofluoresce when calcium binds intracellular calmodulin and emits green fluorescence which was observed over time. Peaks in fluorescence were indicative of intracellular calcium influx. The reduced frequency of calcium influx along with reduced ASM contractions and underdeveloped lungs suggests the mechanism which contributes to respiratory pathologies and poor birth outcomes associated with exposure to arsenic.

Chapter 1

INTRODUCTION

Arsenic, a Historical Perspective

Arsenic is most known for its history as a deadly toxin, and while it has been romanticized by Hollywood films such as “Arsenic and Old Lace,” it is in fact implicated with the death of many actual historical figures (Hughes et al., 2011). Most notably perhaps, is the controversial death of Napoleon Bonaparte, the French military leader who conquered much of Europe in the early 19th century (Hindmarsh & Savory, 2008). In the modern era, however, most of the interest in arsenic toxicology is related to naturally occurring exposure in food, water, and soil (Hughes et al., 2011). Perhaps the most alarming example of natural poisoning, is the mass poisoning of over 80 million citizens of Bangladesh that started in the late 20th century and continues today (Hasan et al., 2019). The majority of people in Bangladesh consume water from wells that are contaminated with high levels of naturally occurring arsenic (Hasan et al., 2019). The citizens of this densely populated third world country are facing severe water pollution (*Arsenic Poisoning in Bangladesh*, n.d.). While almost 97% of the population has access to water, the vast majority of accessible water is contaminated with arsenic as well as other toxic compounds (*WHO, Bangladesh—Sustainable Development & Healthy Environment*, n.d.). Exposure to contaminating drinking water is not isolated to third world countries (*Relation between in Utero Arsenic Exposure and Birth Outcomes in a Cohort of Mothers and Their Newborns from New*

Hampshire, n.d.). In addition to Bangladesh, exposure to arsenic through ground water has been a major public health concern in the United States, Taiwan, Mexico, and India to name a few. (Hasan et al., 2019).

Although arsenic has historically been associated with death and disease, it has also been modified into multiple medicinal therapeutics (Rao et al., 2013). Documented cases of arsenic as a therapeutic agent dates back earlier than 2000 BCE (Hughes et al., 2011). The Father of Medicine, Hippocrates, is thought to have used arsenic paste to treat ulcers and abscesses while other pioneering physicians, such as Aristotle and Paracelsus are also reported to have used arsenic for other medicinal purposes (Hughes et al., 2011). More recently, Fowler's solution was discovered in 1785 and is a 1% solution of potassium arsenite that was used to treat autoimmune diseases of the skin, syphilis, and asthma (Hughes et al., 2011). In 1910, Paul Ehrlich introduced a new, arsenic based drug that was used to successfully treat syphilis until the use of penicillin (Hughes et al., 2011). Derivatives of arsenic have also been used as chemotherapeutics for Cancer since the 1880s. Even today, Arsenic trioxide is used to treat acute promyeloid leukemia (Hughes et al., 2011). While arsenic derivatives are used in medicine, it is important to understand the detrimental implications associated with arsenic exposure in the context of human health

Arsenic is Everywhere

Arsenic is the 20th most common element in the earth's crust and is emitted into the environment as a result of volcanic and industrial activities. (International Agency for Research on Cancer & Weltgesundheitsorganisation, 2012). Arsenic is mainly transported in the environment through water with the form and concentration of arsenic dependent on several factors including whether the water is oxygenated/oxidative state, the type of water source, and the proximity of the water source to arsenic-rich geological formations (International Agency for Research on Cancer & Weltgesundheitsorganisation, 2012). There are many forms of arsenic, with inorganic arsenic compounds being the most toxic (Kuivenhoven & Mason, 2019). Among inorganic arsenic compounds, sodium arsenite predominates in reducing groundwater conditions (International Agency for Research on Cancer & Weltgesundheitsorganisation, 2012). Ground water contaminated with arsenic exceeding 10µg/mL can be found in groundwater around the world (Fig 1). Arsenic is a metalloid element that is usually found in nature in combination with sulfur and other metals (Kuivenhoven & Mason, 2019).

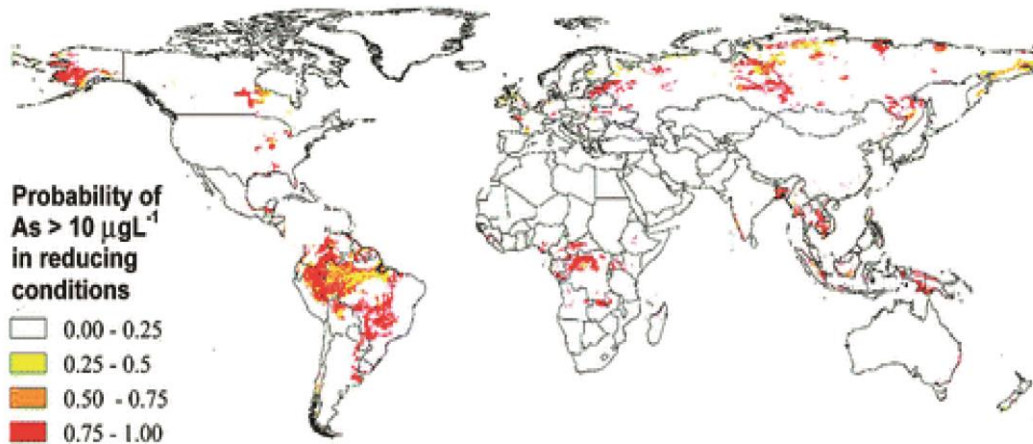


Figure 1. Global Distribution of the Probability of Arsenic Ground Water Contamination. Probability ground water containing >10 $\mu\text{g/mL}$ arsenic for reducing goundwater conditions. Image adapted from Amini et al., 2008

Over 100 million people world-wide are exposed to arsenic, mostly through contaminated ground water that is either directly consumed or used to grow crops (*Arsenic Poisoning in Bangladesh*, n.d.). Exposure can also occur to developing fetuses when arsenic travels through the placental barrier when a mother consumes food or water that is contaminated with arsenic (Wai et al., 2017).

When exposure occurs, absorption occurs predominantly through ingestion via the small intestine, and minimal absorption occurs from skin contact and inhalation (Ratnaik, 2003). When arsenic is absorbed, it undergoes hepatic processing to change it to a less toxic, and excretable form, but it is not at all innocuous (Ratnaik, 2003). About 50% of the ingested dose may be eliminated in the urine in three to five days after absorption with urinary concentration of arsenic being the most accurate measurement reflecting the amount of arsenic that was ingested (Ratnaik, 2003). Acute arsenic poisoning results in a high concentration of arsenic in the liver and

kidneys while chronic arsenic ingestion leads to additional accumulation in the heart and lungs (Ratnaïke, 2003).

The human health implications associated with arsenic exposure are huge, and with so many people being exposed through drinking water, contaminated crops, and through placental transfer, it is critical that we understand how exactly arsenic exposure affects human health. The vast majority of related research has been conducted to examine adult exposure, leaving a paucity of research related to how arsenic affects embryonic development. While the risks associated with in utero exposure have become increasingly appreciated, little is known regarding the mechanism of how arsenic affects development.

Arsenic and Pathology

Post-natal exposure to arsenic has been linked to many health concerns including skin disorders, reduced skeletal muscle function, lung cancer, heart disease, and high blood pressure to name a few (Ratnaïke, 2003). Non-malignant respiratory defects are also associated with arsenic exposure including Chronic Obstructive Pulmonary Disease (COPD), respiratory failure, and pulmonary edema (Ratnaïke, 2003). Clinical features of arsenic exposure differ with regard to the length of exposure (Table 1) (Ratnaïke, 2003). Acute arsenic toxicity is associated with nausea, vomiting, abdominal pain, and

severe diarrhea in addition to more severe symptoms include acute psychosis, diffuse skin rash, fatal cardiomyopathies, and seizures (Ratnaike, 2003). Chronic arsenic toxicity on the other hand, manifests features including malignant changes in almost all organs of the body, and an increased risk for diseases including cardiovascular disease, peripheral vascular disease, respiratory disease, diabetes mellitus, and neutropenia. (Ratnaike, 2003). Of particular relevance to this research are the respiratory defects associated with exposure to arsenic.

Table 1.1 Complications of Arsenic Exposure (Acute vs Chronic)

Complications of Arsenic Exposure (Acute vs Chronic) Adapted from Ratnaike et al., 2003 and Singh et al., 2011	
Acute Arsenic Exposure	Chronic Arsenic Exposure
<ul style="list-style-type: none"> • Respiratory failure • Renal failure • Acute psychosis • Encephalopathy • Cardiomyopathy • Seizures 	<ul style="list-style-type: none"> • Accumulation in lungs, heart, liver, kidneys, muscles, nervous system, gastrointestinal tract, spleen • Malignancies of the lung (and nearly all other organ systems) • Increased risk for non-malignant respiratory disease (Asthma, Respiratory failure, Chronic Obstructive Pulmonary Disease) • Increased risk for cardiovascular disease, Parkinson’s Disease, and Diabetes Mellitus • Skeletal and vascular muscle dysfunction

While the symptoms of acute and chronic adult exposure are well characterized, little is documented regarding symptoms of in utero exposure. In utero exposure to arsenic occurs from a mother to her baby via trans-placental transport (Gerber et al., 1982).

Although the placenta may act as a selective transporter that prevents the passage of potentially toxic substances to the developing fetus, some environmental contaminants can freely or partially cross the placental barrier (Needham et al., 2011). In particular, environmental heavy metals such as arsenic, cadmium and lead are known to increase health risks to infants through trans-placental transport (Wai et al., 2017). Compared to women who were not exposed to arsenic, adverse pregnancy outcomes in terms of spontaneous abortion, stillbirth, and preterm birth rates are significantly higher among women who are exposed to chronic arsenic exposure through contaminated drinking water (Ahmad et al., 2001). While studies have correlated poor birth outcomes with mothers who have been exposed to arsenic, little is known about the specific molecular mechanism pertaining to arsenic-induced pathologies that originate from utero exposure (Singh et al., 2011).

Arsenic has body wide, multi-system toxicities, the specifics of which have left researchers and physicians with a lot to learn. There are however several proposed mechanisms for how arsenic exerts its toxic effects for disorders such as diabetes, certain cancers, cardiovascular disease, and neurological disorders (Singh et al., 2011).

Arsenic exerts its toxicity by increasing reactive oxygen species, forming ADP-Arsenate, and increasing calcium sensitivity. Increasing reactive oxygen species leads to oxidative damage to DNA, a precursor to many cancers, and regulation of transcription factors related to impairment in cognitive function (Hajjar et al., 2018).

It also interferes with phosphate groups present in various enzymes involved in glucose metabolism including pyruvate dehydrogenase and glucose transporters, contributing to impaired enzyme function (Kulshrestha et al., 2014). The expression of genes involved in glucose metabolism are then altered, ultimately further stimulating oxidative stress. (Kulshrestha et al., 2014)

Arsenic is known to inactivate over 200 enzymes, most notably are those involved in cellular survival pathways and DNA replication and repair (Singh et al., 2011). The capability of arsenic to inactivate enzymes contributes to its toxicity, but it is also this property that provides arsenic its cancer therapeutic potential. (Chou et al., 2001).

Arsenic inhibits the activity of telomerase, the enzyme responsible for improving chromosomal stability via the addition of telemeric repeats to the end of chromosomes (Chou et al., 2001). This phenomenon explains the seeming contradictory carcinogenic properties of unbound arsenic and anti-tumor properties of arsenic-based cancer therapeutics. (Chou et al., 2001).

A mechanism for arsenic-induced neurotoxicity has also been proposed (Figure 2).

Due to the fact that arsenic freely crosses the blood-brain barrier, exposure is associated with a wide range of neurological complications including impaired memory, impaired concentration, and Parkinson's disease (Singh et al., 2011). The mechanism proposed also largely involves oxidative stress and alterations in

metabolism of various neurotransmitters such as monoamines and acetylcholine (Singh et al., 2011).

Correlations linking arsenic exposure to cardiovascular diseases including atherosclerosis, hypertension, and ventricular arrhythmias have also been documented. (Singh et al., 2011). Arsenic stimulates nicotinamide adenine dinucleotide phosphate (NADPH) oxidase in the plasma membrane of vascular endothelial cells and vascular smooth muscle cells to increase the generation of reactive oxygen species (ROS) (Singh et al., 2011). ROS couples with nitric oxide to form a strong oxidant implicated with the upregulation of inflammatory intermediates and the increase of the expression of atherosclerosis-related genes (Singh et al., 2011). Arsenic also mediates vasoconstriction of the blood vessels by promoting the phosphorylation of myosin light chain kinase (MLCK) and increasing calcium sensitization leading to hypertension (Singh et al., 2011). Chronic exposure to oxidative stress alters the release of vasoactive mediators in the blood which also contributes to the elevation of blood pressure (Figure 2) (Singh et al., 2011).

Arsenic inactivates many enzymes by binding thiol or sulfhydryl groups in proteins of the liver, lungs, kidney, spleen, and GI tract, thus contributing to system wide pathologies; an important property to note considering the available treatments for arsenic exposure (Ratnaike, 2003). Current treatment for arsenic exposure includes symptom management/ treatment of specific organs or systems that have been affected

(Kosnett, 2013). Aside from symptom management, chelation agents are the only other treatment for acute arsenic exposure (Kosnett, 2013). Chelation therapy was originally developed in the late 1950's in response to an arsenic-based warfare agent and has remained the mainstay treatment for arsenic poisoning to this day (Kosnett, 2013). Working from the knowledge that arsenic formed complexes with enzymes by reacting with thiol groups, researchers developed a thiol compound as an antidote. Chelation therapy is efficacious as it competes for the thiol binding sites of arsenic, preventing arsenic from forming complexes with the thiol groups of endogenous enzymes (Kosnett, 2013).

Although chelation following exposure to inorganic arsenic may accelerate excretion and diminish burden in some organs, potential therapeutic efficacy in terms of decreased morbidity and mortality is largely unestablished in cases of chronic metal intoxication. (Kosnett, 2013). There are no additional evidence-based treatments for chronic arsenic poisoning, thus, toxicity management strategies continue to focus on reducing arsenic ingestion and treating the presenting symptoms (Ratnaike, 2003).

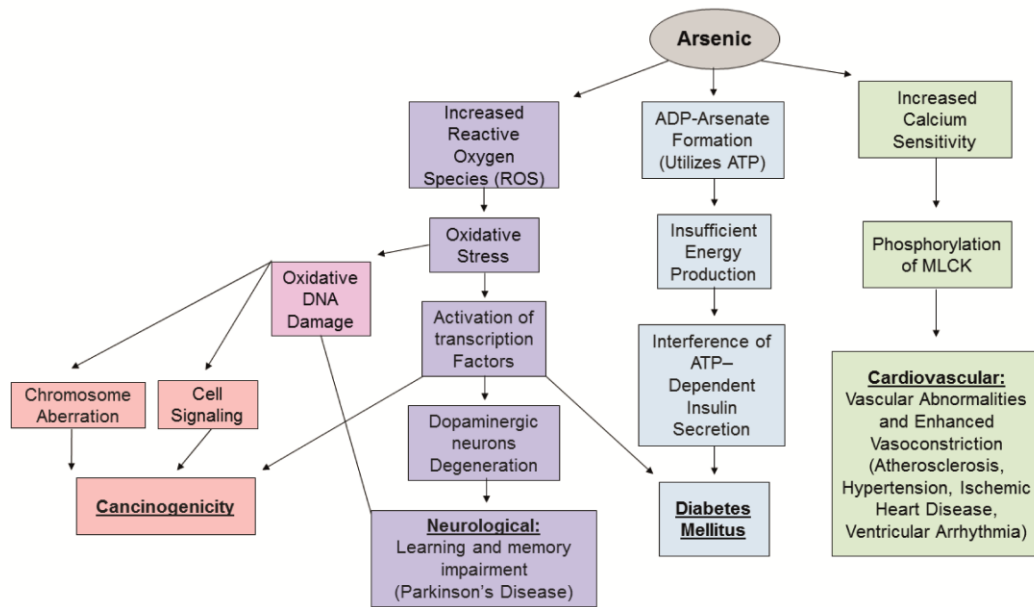


Figure 2. Proposed Mechanisms for Common Arsenic-Induced Pathologies

Pathways have been proposed for some of the major diseases associated with arsenic exposure, but the pathway leading to respiratory dysfunction remains unknown. Like mechanisms underlying arsenic-induced lung pathology, a gap in knowledge exists in understanding the impact of arsenic exposure on fetal development, despite the knowledge that arsenic travels from mother to baby through trans-placental transport (Gerber et al., 1982). Of the studies related to arsenic and poor birth outcomes, many are large population studies that aim to show the correlation of arsenic-exposed pregnant mothers and birth outcomes rather than understanding the molecular mechanisms underlying the health concerns, thus there is a critical need to understand how arsenic affects embryonic lung development.

Lung Development

Asthma, COPD, lung cancer, and respiratory distress mouse models have all been used to study human respiratory pathology (Ghorani et al., 2017). Lung development and maturation has been divided into four stages: pseudoglander, canalicular, terminal saccular, and alveolar. (Warburton et al., 2010). Both human and mice follow the same order of lung development (Table 2), one of the many reasons the mouse model is an appropriate model and the simplest model for studying human lung development. (Warburton et al., 2010).

Mouse embryonic lung development begins by invagination of the laryngeal-tracheal groove from the foregut endoderm at embryonic day 9.5 (E9.5) (Rankin & Zorn, 2014). Various growth factors, including those from the epidermal growth factor (EGF), fibroblast growth factor (FGF), sonic hedgehog (SHH), bone morphogenetic protein (BMP), and wingless (Wnt) signaling families, are required for regulation of respiratory organogenesis (Rankin & Zorn, 2014). Many of these growth factors have been extensively studied and affect epithelial branching, proliferation, and differentiation (Rankin & Zorn, 2014).

At embryonic day 13 (E13), the lungs are easily imaged and well stereotyped as the lungs have not had extensive development to the point that the 3D structure is overly intricate and there is minimal variation among different embryos (Metzger et al., 2008).

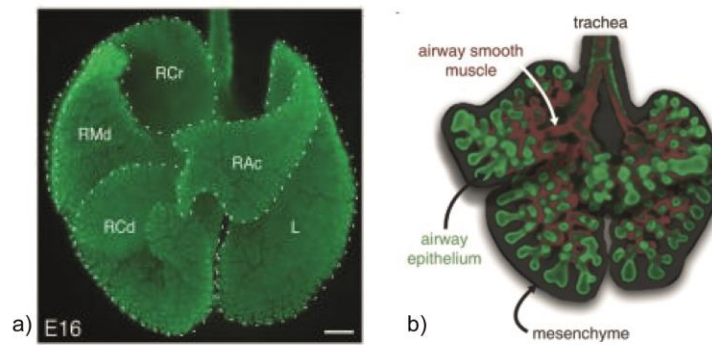


Figure 3. Architecture of the Developing Embryonic Mouse Lung. a) E16 mouse lung immunostained for E-Cadherin. Lobes of the lung are labeled: right cranial lobe (RCr), right medial lobe (RMd), right caudal lobe (RCd), right accessory lobe (RAc), and left lobe (L). Adapted from Metzger et al., 2008. b) E13 Mouse lung. Airway epithelium (green) is surrounded by mesenchyme (gray), and airway smooth muscle (red) wraps around epithelial branches. Adapted from Nelson et al., 2017.

Tissue layer similarities among humans and mice are also apparent (Warburton et al., 2010). In both humans and mice (Table 2), bronchial branches arise initially as two distal buds, with each bud consisting of three different layers: the epithelium, the surrounding mesenchyme, and the mesothelium (del Moral and Warburton 2010). (Figure 3,5). The epithelium can be visualized via E-Cadherin (ECAD) immunostain (Figure 3) or by bright field imaging of whole lung explants (Figure 5).

ECAD is an epithelial adhesion molecule and part of the cadherin family of transmembrane-associated glycoproteins that mediate specific cell-cell adhesion (van Roy & Berx, 2008). It is expressed in all mammalian epithelia and is important for establishing apicobasal polarity, preserving epithelial cell survival, and controlling cell proliferation (van Roy & Berx, 2008). ECAD is present in the developing embryo as

early as the 4-cell stage and persists in the epithelium of adult tissues (Wu et al., 2010). During lung development, ECAD is present in the epithelia of the primary pulmonary primordium, the secondary bronchi, and the adult bronchial epithelium, making it a good candidate protein for identifying airway epithelium in embryonic lungs and throughout development (van Roy & Berx, 2008). Immunostaining for ECAD is a reliable method for visualizing the airway architecture of E13 mouse lungs. (Figure 3) (Metzger et al., 2008).

In the embryonic mouse, neural crest-derived cells (NCC) that will differentiate into neurons and glia of the nervous system are already present when the lung buds arise at embryonic Day 9.5 (Tollet et al., 2002), and it is assumed that some of these cells will migrate into the lung as it is forming. At E12, nerve trunks mainly follow the airway tubules which are covered by airway smooth muscle, to the base of the epithelial buds, and by E13 some nerves extend out into the mesenchymal cap beyond the buds. (Tollet et al., 2002).

In arsenic-induced cardiovascular pathologies, dysfunction of vascular and cardiac smooth muscle contributes to the severity of diseases such as hypertension, ischemic heart disease, and cardiac dysrhythmias (Singh et al., 2011). It is fair to question if arsenic also has an effect on the smooth muscle of the airways. Also, correctly functioning airway smooth muscle has been implicated in the branching pattern of the developing embryonic lung (Nelson et al., 2017).

Table 2.1 Stages of Lung Development (Human vs Mouse)

Table 2. Stages of Lung Development (Human vs Mouse) Adapted from Warburton et al., 2010			
Stage of Development	Developmental Processes	Age of Gestation (Human)	Age of Gestation (Mouse)
Pseudoglandular	<ul style="list-style-type: none"> • Epithelial tubes undergo branching morphogenesis. • Primitive respiratory tree is too immature to support gas exchange • Airway smooth muscle develops and surround major airways 	5-17 weeks of pregnancy	Embryonic day 9.5 (E9.5)-E16.6
Canalicular	<ul style="list-style-type: none"> • Respiratory tree is expanded in diameter and length • vascularization and angiogenesis begin • Terminal bronchioles divide into respiratory bronchioles and alveolar ducts 	16-25 weeks of pregnancy	E16.6-E17.4
Terminal Saccular	<ul style="list-style-type: none"> • Interstitium thins due to apoptosis and differentiation of mesenchymal cells • Alveolar epithelial cells differentiate and bear lamellar bodies that contain surfactant • Extensive network of capillaries is expanded • Fetal lung can support air exchange in prematurely born human neonates 	24 weeks to late fetal period	E17.4- post natal day 5 (P5)
Alveolar	<ul style="list-style-type: none"> • Alveolarization occurs and the majority of gas surface exchange is formed 	Late fetal to childhood	P5-P30

Adult mammalian lungs are branched networks of airways organized in intricate patterns (Metzger et al., 2008). In addition to tissue layer organization, lung architecture among humans and mice is also comparable in that there are 5 lung lobes at the completion of lung development (Warburton et al., 2010). In humans, three lobes form on the right side and two lobes on the left side while in mice, four lobes form on the right (cranial, medial, and caudal lobes, plus the accessory lobe) and one on the left (Figure 3) (Warburton et al., 2010). The 3-dimensional pattern of branching has been reconstructed and is remarkably stereotyped in the embryonic mouse lung (Fig 4) (Metzger et al., 2008). The same sequence of branching events occurs in every embryo with the major airways including the trachea and bilateral bronchi developing first followed by branching that occurs in the proximal to distal direction (Figure 4a) (Metzger et al., 2008). Each branching event can be categorized as either terminal bifurcation or domain branching. When bifurcation occurs, a branch is split into two daughter branches whereas domain branching generates new buds off of the side of an existing parent branch (Figure 4b) (Metzger et al., 2008).

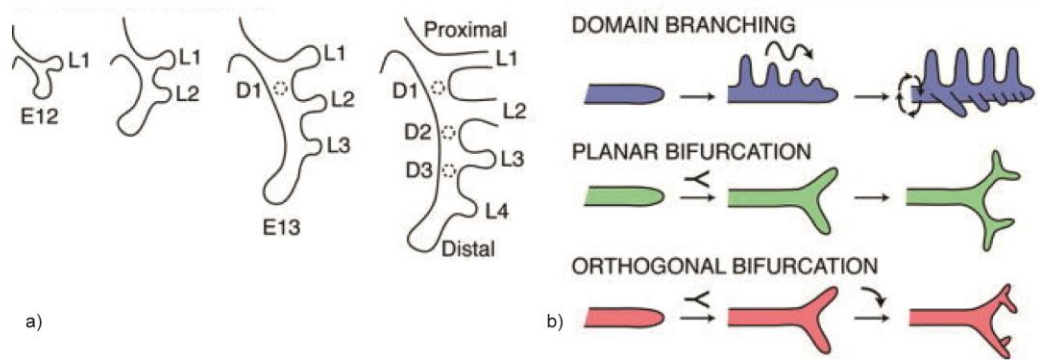


Figure 4. Branching Morphogenesis of the Developing Embryonic Lung. a) Schematic of lateral (L) and dorsal (D) secondary lateral branches (L1-5) budding from the left lobe in a proximal to distal order. Proximal to distal branching also occurs as secondary dorsal branches form (D1-3; dashed circles). b) Schematic of branching modes. Schematics show patterning of morphogenesis of new branches for each mode: domain branching, planar branching, and orthogonal bifurcation. Adapted from Metzger et al., 2008.

Pre-term infants have an increased risk for underdeveloped lungs and likely have an even higher risk if exposed to arsenic in utero considering its link to lung defects and respiratory pathology including COPD and Asthma (Hilgendorff et al., 2014). These respiratory diseases have an airway smooth muscle component that contributes to the severity of the disease (Lambert et al., 19910), thus understanding how arsenic affects smooth muscle would shed light on the mechanism behind arsenic-induced respiratory pathologies associated with in utero exposure.

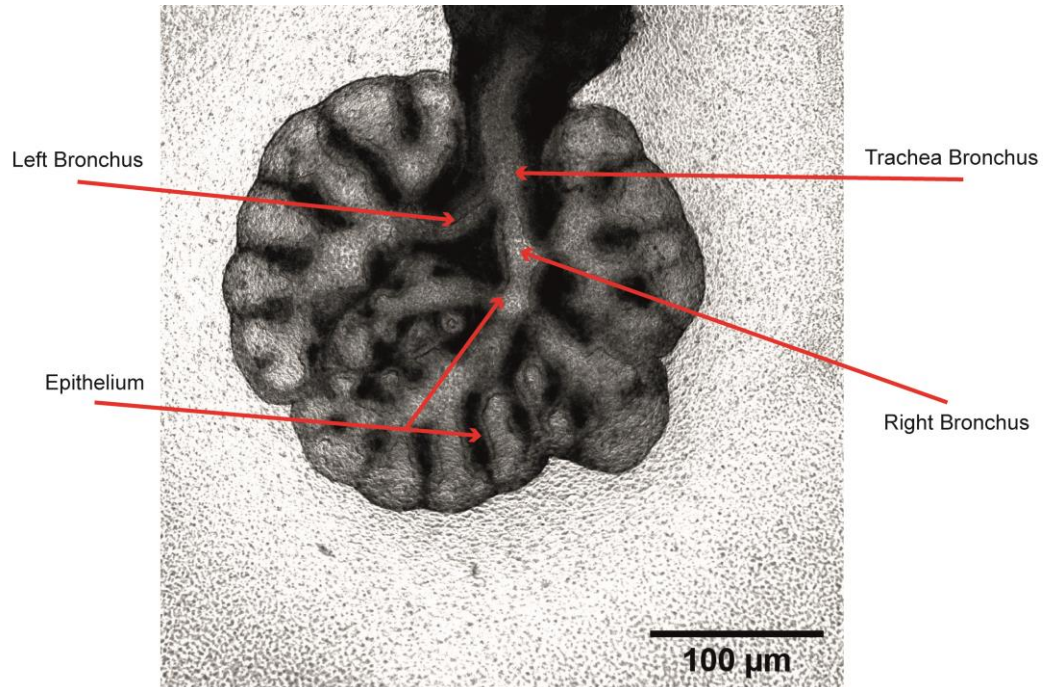


Figure 5. Brightfield Image of Whole Explant Lung. Bright field image of an E13 CD1 whole lung explant focused on the epithelium. Red arrows indicate major airways and airway epithelium.

Airway Smooth Muscle and Its Role in Development

Knowing that arsenic has molecular interactions with vascular and cardiac smooth muscle, a possible mechanism is suggested implicating airway smooth muscle as a target arsenic-induced lung pathology (Lee et al., 2005).

A layer of mesenchymal-derived smooth muscle develops concomitantly with the airway epithelium (Goodwin et al., 2019). ASM cells that encircle the airways relocate around the epithelium as it extends distally (Goodwin et al., 2019). At E10.5, cartilage is observed around the upper airways (trachea and bronchi), and by E 11.5, smooth muscle is present and localized to the medial half of the bronchi (Hines et al., 2013).

Airway smooth muscle can be visualized using a variety of methods including immunofluorescent microscopy of tissue sections and whole lung explants (Figure 3) (Nelson et al., 2017).

The pattern of airway domain branching of embryonic mouse lungs is highly stereotyped, as is the pattern of smooth muscle that differentiates around the base of each branch (Figure 4) (Metzger et al., 2008, McCray, 1993). The dysfunction of ASM in adult respiratory pathologies is well characterized (An et al., 2007), but ASM's role in development is not. It is known however, that perturbing the pattern of smooth muscle differentiation causes abnormal domain branching, that epithelial proliferation alone is insufficient to generate domain branching, and that smooth muscle wrapping is required to shape the epithelium into a branch (Goodwin et al., 2019). Although ASM contractile activity is implicated in numerous respiratory pathologies, little else is known regarding the role of ASM in development (Schittny et al., 2000).

Interestingly, spontaneous contractions of ASM in early embryonic development have been observed across mammalian models including human, mouse, rabbit, pigs, and Guinea pigs (McCray, 1993). Spontaneous ASM contractions are an observed and well recognized developmental phenomenon, but are poorly characterized (Nakamura & McCray, 2000). In utero exposure to arsenic may contribute to poor birth outcomes

and respiratory disease by modulating the airway smooth muscle contractions that occur during development.

The narrowing of the airways caused by contractions in ASM can be characterized as being either tonic or phasic in nature (Zhang et al., 2010). Post-natal ASM contractions are characterized as tonic due to the fact that they are similar to that of the vascular smooth muscle in blood vessels and characterized by slow, graded contractions that lead to airway narrowing whereas pre-natal ASM contractions are characterized as phasic due to their similarity to gastrointestinal smooth muscle contractions (Schittny et al., 2000). During development or at birth, ASM loses the capacity to generate spontaneous electrical activity thus losing its ability to spontaneously contract, and acquires the characteristics of tonic smooth muscle (Schittny et al., 2000).

During embryonic branching morphogenesis, a simple cluster of cells proliferates, and propagating waves of phasic ASM contractions travel proximal to distal (Figure 5) facilitating the flow of fluid through the lungs and the supporting the generation of a branched network of airways (Nelson et al., 2017). These ASM contractions can be visualized using brightfield time lapse imaging and analyzed in a variety of ways (Figure 12 (Nelson et al., 2017)). The contractions cause visible movement of intraluminal fluid and distension at the distal ends of epithelial tubules, suggesting that they produce significant changes in intraluminal pressure (McCray 1993). As the

contractions proceed distally, toward the terminal tubules, buds expand suggesting a role of ASM in branching morphogenesis. (Nelson et al., 2017).

Arsenic has been shown to interact with cardiac smooth muscle contributing to the correlation of arsenic exposure and the increased risk of diseases including atherosclerosis, hypertension, and peripheral vascular disease (Figure 2) (Singh et al., 2011). Arsenic stimulates enzymes in the plasma membranes of vascular smooth muscles cells that increase the generation of ROS leading to inflammation and the increase of atherosclerosis-related genes expression (Singh et al., 2011). Arsenic also leads to constriction of the blood vessels by promoting the phosphorylation the contraction regulatory molecule myosin light chain kinase (MLCK) and increasing calcium sensitization (Singh et all., 2011). Given the similarities between the developing ASM and the contraction of vascular smooth muscle, this mechanism is a likely candidate for how arsenic contributes to respiratory pathologies involving ASM.

Regulation of Airway Smooth Muscle Contraction

ASM contracts when the thick filaments of myosin motors interact with the thin filaments of actin thus shortening individual myocytes (Lavoie et al., 2009). Actin filaments are interconnected and oriented along the axis of each myocyte, thus allowing for entire muscular tissues to be contracted when myocytes that share axis orientation contract in concert (Figure 7) (Lavoie et al., 2009). Both tonic and phasic

smooth muscle contraction share some common regulatory signaling pathways centered on the molecular motor myosin as well as the influx of intracellular calcium (Zhang et al., 2010).

A major determinant of the contractile property of smooth muscle cells is the extent to which actomyosin cross-bridge interactions form (An et al., 2007). Sustained high levels of cross-bridge formation lead to muscle contraction while low levels allow for muscle relaxation (An et al., 2007). The rate of cross-bridge activity depends on the phosphorylation state of the regulatory molecule myosin light chain (rMLC) (An et al., 2007). The activity of MLC is determined by the opposing activities of myosin light chain kinase (MLCK) and myosin light chain phosphatase (MLCP) (An et al., 2007). While MLCK activity is generally regulated by intracellular Ca^{2+} concentration, MLCP activity is a complex result of the activity of a variety of kinases.

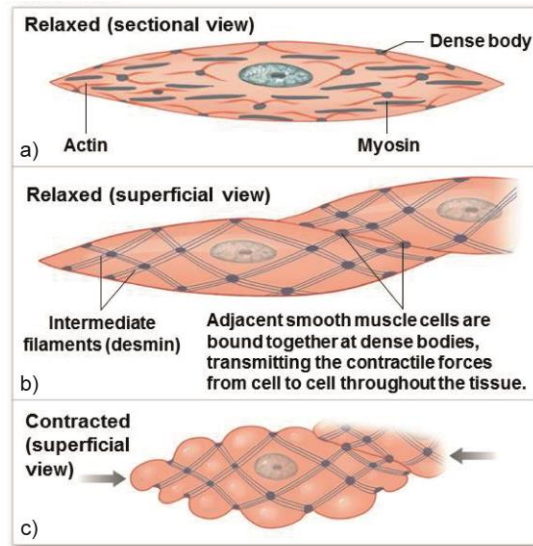


Figure 6. Smooth Muscle Contraction. a) Sectional view of a relaxed smooth muscle cell (myocyte). Actin (thin filaments) and myosin (thick filaments) are oriented along the axis of the cell and scattered throughout the cytoplasm. b) Superficial view of relaxed smooth muscle cells connected together at dense bodies allowing contractile forces to travel from one cell to another throughout the muscle tissue. c) Superficial view of a contracted muscle cell. Myosin-mediated modifications of actin thin filaments shorten individual myocytes, allowing whole muscular tissues to contract when myocytes that share an axis contract in concert (Lavoie et al., 2009). Image adapted from Smooth Muscle, n.d.

While MLCK activity is generally a function of the intracellular Ca^{2+} concentration, MLCP activity is a complex result of the activity of a variety of kinases and phosphatases, and in most cases, is independent of Ca^{2+} concentration (An et al., 2007). This ability of the smooth muscle cell to modulate MLCP activity independently of the Ca^{2+} -dependent MLCK activity is referred to as Ca^{2+} sensitivity (An et al., 2007). When intracellular calcium increases, so does the amount of rMLC phosphorylation leading to an increase in ASM contraction (An et al., 2007).

Arsenic mediates vascular smooth muscle contractions by modulating molecules in this pathway (Singh et al., 2011). It increases calcium sensitivity thus increasing activity of MLCK and inducing hypercontraction (Singh et al., 2011). This suggests

that arsenic may modulate airway smooth muscle contraction via calcium sensitivity and/or regulation of MLC phosphorylation leading to respiratory system disease.

Calcium/Calmodulin-Mediated Contractile Regulation Pathway

Arsenic contributes to cardiac disease by interacting with molecules in the calcium/calmodulin pathway that regulate muscle contractions by altering the phosphorylation levels of MLC (Singh et al., 2011). In vascular smooth muscle, hypercontraction by arsenic correlates with the extent of MLC phosphorylation (Singh et al., 2011). Arsenic enhanced vasoconstriction without an increase in intracellular calcium levels suggesting that for vascular smooth muscle, calcium sensitization plays a role in abnormal contractile phenotypes. These molecules are also important for the regulation of ASM (Ammit et al., 2000). Arsenic may contribute to respiratory pathologies related to ASM by interacting with molecules in the calcium/calmodulin pathway like it does for cardiovascular diseases of the smooth muscle.

When intracellular calcium increases, it binds to calmodulin which in turn phosphorylates and activates MLCK. When MLCK is activated, it phosphorylates rMLC allowing it to interact with the actin molecules in the muscle cells. Intracellular calcium levels are modulated through various pathways (Figure 7). Cholinergic receptors are activated by the endogenous agonist Acetylcholine (Ach) (Bergner & Sanderson, 2002). Ach acts on M2 and M3 cholinergic receptor subtypes to elicit a calcium response (Figure 8) (Jude et al., 2008). The M3 receptor subtype is coupled to

a $G\alpha_q$ protein which recruits phospholipase C- β (PLC- β) and generates inositol 1,4,5-tris-phosphate (IP3) (Jude et al., 2008). IP3 acts on the IP3-receptor to increase its probability of releasing calcium from the sarcoplasmic reticulum (SR) into the cytoplasm (Fig 8) (Jude et al., 2008). When the M2 receptor subtype, which is coupled to $G\alpha_i$, is activated, a signaling pathway involving the ADP ribosyl cyclase CD38 is initiated which leads to the generation of cyclic adenosine diphosphate ribose (cADPR), an endogenous calcium mobilizing nucleotide (Wei et al., 2014). cADPR generated by CD38 is transported back into the myocyte, and ADPR acts on transient receptor potential (TRP) channels to elicit an influx of divalent ions including calcium (Jude et al., 2008). Sarcoplasmic reticulum calcium-ATPase (SERCA2) pumps cytosolic calcium back into the SR to replenish the SR calcium store when they become depleted (Fig 8) (Jude et al., 2008).

Calcium influx from the extracellular space via voltage and receptor gated channels is critical for the repletion of intracellular calcium stores (Jude et al., 2008). Studies show that fetal lung slices exhibit increased contractions with acetylcholine treatment and inhibited contraction with calcium channel blockers (Bergner & Sanderson, 2002).

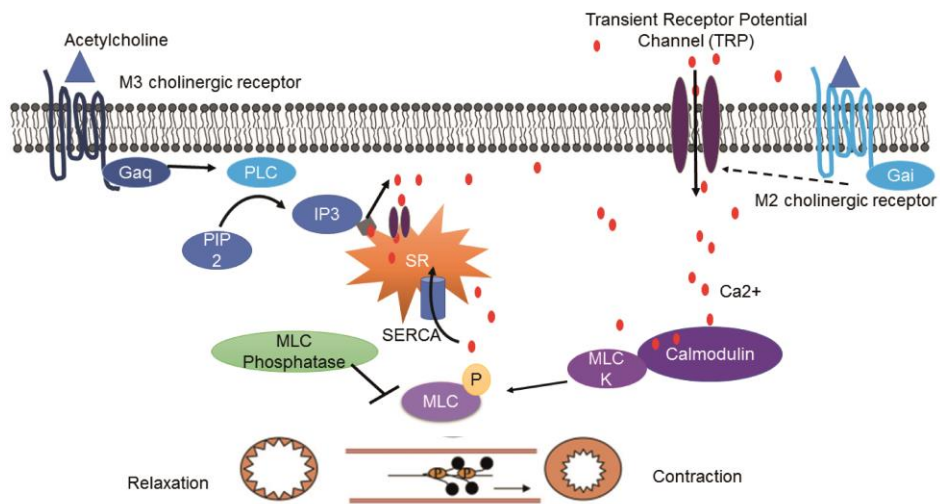


Figure 7. Regulation of Airway Smooth Muscle Contraction. Acetylcholine (Ach) acts on M2 and M3 cholinergic receptors subtypes to elicit a calcium response. M3 receptor subtype is coupled to a Gαq subunit which recruits phospholipase C (PLC) and generates 1,4,5-tris-phosphate (IP3) that acts on the IP3-receptor (IP3R) to increase its probability of releasing Ca²⁺ from sarcoplasmic reticulum (SR) into the cytoplasm. M2 receptor subtype is coupled to a Gαi subunit leads to activation of transient receptor potential (TRP) channels to elicit an influx of divalent cations including Ca²⁺. Dotted line from M2 cholinergic receptor to calcium influx through TRP channel represents steps in signaling that are not shown (M2 subtype receptor activates CD38/cADPR signaling pathway). SR Ca²⁺-ATPase (SERCA) pumps cytosolic Ca²⁺ back into the SR to replenish SR calcium stores. Increased levels of intracellular calcium lead to phosphorylation of the myosin light chain (MLC), initiating smooth muscle contractions. myosin light chain phosphatase removes phosphate from MLC to stop contractions. Figure adapted from Jude et al., 2008.

ACH-induced contractions accompany a transient increase in calcium in individual ASM cells that subsequently declines to initiate multiple intracellular calcium oscillations (Bergner & Sanderson, 2002). Exposure of ASM to contractile agonists results in a biphasic elevation of intracellular calcium concentration that is characterized by an initial rapid and transient rise in calcium, followed by a decline to a lower, sustained steady-state concentration (Jude et al., 2008). This biphasic response results from calcium influx from the extracellular space and release of calcium from the intracellular stores of the SR (Jude et al., 2008).

Analysis of the involvement of arsenic in airway smooth muscle will give insight into the mechanism for which it contributes to respiratory pathologies involving ASM and in utero exposure. This research aims to determine if arsenic exposure affects embryonic lung function by modulating airway smooth muscle contractions via the calcium/calmodulin mediated pathway.

To study the effect of arsenic, ASM contraction frequency, α -smooth muscle actin (α -AMA) abundance, and calcium signaling characteristics are studied. Embryonic lungs are isolated from pregnant mice and cultured in the presence or absence of arsenic to determine the effect of arsenic exposure to the developing lung. These lungs are then able to be imaged to observed airway smooth muscle contractions to determine if exposure results in a change in the contraction frequency. Immunofluorescence is also performed on these lungs to visualize structural features including the epithelium and smooth muscle (visualized with α -SMA) to compare the airway architecture of treated and untreated lungs as well as the appearance and location of α -SMA. The α -SMA in the lungs is also quantified by western blot to determine the relative abundance in untreated and treated lungs. Finally, lungs are isolated from transgenic mice and imaged to allow the visualization of calcium signaling events. These events are quantified and the relative frequency of calcium signaling events. Together, the results of this study will elucidate the mechanisms underlying lung pathologies associated with arsenic exposure.

Chapter 2

MATERIALS AND METHODS

Overall Study Design

The aim of this research was to test the effects of arsenic on embryonic lung development. E13 mouse lungs were cultured in standard explant media (control) or media containing 0.1, 0.5, and/or 1ng/mL sodium arsenite for 24 hours and data was collected. Media and treatment were changed every 24 hours to ensure consistent dosing of sodium arsenite and nutrients for longer duration experimentation.

CD1 mouse lungs were used for assays including lung structure analysis, western blot, and contraction analysis. Lung structure analysis was performed to test the effects of arsenic on the width of major airways of the lung as well as the thickness of smooth muscle along the bronchi and samples were collected, fixed, and immunostained after 24 hours in culture. Western blot was performed to quantify the amount of α -SMA in the lungs and samples were also collected and lysed 200 μ L radio immunoprecipitation assay (RIPA) lysis buffer (Alfa Aesar) containing Halt Protease and Phosphatase Inhibitor (Thermo Scientific) at 24 hours in culture. Contraction analysis of CD1 lungs tested the effect of arsenic on ASM contractions. Samples were imaged for a total of 24 hours starting at 24 hours in culture and proceeding until 48 hours in culture.

GCaMP mouse lungs were used for calcium/calmodulin signaling analysis and corresponding contraction analysis. Green fluorescence channel imaging was started at 24 hours in culture to analyze calcium/calmodulin binding-induced fluorescence followed by brightfield time lapse imaging to analyze the frequency of contractions in these lungs.

CD1 Mouse and GCaMP Transgenic Mouse

Animals were housed at the University of Delaware Life Sciences Research Facility. Mice were euthanized by CO₂ asphyxiation, confirmed by cervical dislocation, and uteri were then isolated.

CD1 mice were received from Charles River Laboratory under the Animal Use Protocol approved by the Institutional Animal Care and Use Committee (IACUC) at the University of Delaware (AUP #1320). The progenitors of this CD1 stock consisted of 2 male and 7 female albino mice derived from a non-inbred stock in Switzerland. These animals were imported into the US in 1926 and today, Charles River labs use their International Genetic Standardation (IGS) system to minimize inbreeding and manage random genetic drift.

Acta2^{BAC}-GCaMP-GR (GCaMP) mice were received from The Jackson Laboratory under IACUC-approved protocol (AUP #1320). GCaMP transgenic mice are a fluorescent calcium indicator strain that exhibits high calcium-sensor expression in smooth muscle actin (*025406—B6;FVB-Tg(RP23-370F21-GCaMP3*/mCherry)1Mik/J*, n.d.). The ratiometric GCaMP-Green/Red (GR) allows calcium-independent bright mCherry fluorescence to occur when enhanced green fluorescence protein (EGFP) fluorescence is dim (before calcium binds), and increased EGFP fluorescence upon calcium binding, when the pore in GCaMP becomes occupied (*025406—B6;FVB-Tg(RP23-370F21-GCaMP3*/mCherry)1Mik/J*, n.d.). The calcium indicator is under the control of the Acta2 locus promoter/enhancer region within the BAC transgene. In the absence of calcium binding, bright mCherry fluorescence and low/baseline EGFP fluorescence is observed (*025406—B6;FVB-Tg(RP23-370F21-GCaMP3*/mCherry)1Mik/J*, n.d.). Following calcium binding (such as during muscle contraction), bright EGFP fluorescence is observed (*025406—B6;FVB-Tg(RP23-370F21-GCaMP3*/mCherry)1Mik/J*, n.d.).

The calcium indicator GCaMP-GR is a GCaMP3 variant (GCaMP3 is the first GFP-based calcium sensor for imaging calcium dynamics) fused to the mCherry fluorescent protein by a flexible alanine-proline repeat linker (*025406—B6;FVB-Tg(RP23-370F21-GCaMP3*/mCherry)1Mik/J*, n.d.) . Compared to GCaMP3, GCaMP-GR has equivalent calcium sensitivity, lower resting fluorescence, and higher dynamic range and calcium independent mCherry fluorescence (*025406—B6;FVB-Tg(RP23-370F21-GCaMP3*/mCherry)1Mik/J*, n.d.). This allows for calcium-independent mCherry fluorescence before calcium transients when GCaMP fluorescence is dim as GCaMP has a pore from the outside of its barrel into the chromophore (*025406—B6;FVB-Tg(RP23-370F21-GCaMP3*/mCherry)1Mik/J*, n.d.). Upon calcium binding, this pore becomes occupied and EGFP fluorescence is increased (*025406—B6;FVB-Tg(RP23-370F21-GCaMP3*/mCherry)1Mik/J*, n.d.).

Ex Vivo Lung Culture

Timed-pregnant mice were sacrificed 13 days after breed by CO₂ asphyxiation confirmed by cervical dislocation according to University of Delaware IACUC guidelines. After sacrifice, the pregnant female was submerged in 70% ethanol and an incision was made in the abdomen to expose the uterus which was then removed. The uterus was placed in a Petri dish with 50mL of ice-cold phosphate buffer solution (PBS) + 1% Penicillin Streptomycin Solution (Corning). The Petri dish was then placed under a stereoscopic dissecting microscope and the embryos were removed from the uterus by incising the uterine wall with dissection forceps (Dumostar Dumont Tweezers #4). Embryonic lungs were isolated from each embryo (Figure 8). The embryo was placed on its left side (Figure 8a,b) and the top half of the head was removed. The bottom half of the body was removed above the lower hind limb buds. The spine and posterior tissue were removed, and the embryo was placed in prone position. The aorta and any remaining back tissue were removed to expose the lungs (Figure 8d). The neck was then opened to reveal esophagus and trachea. The esophagus was removed allowing for the isolation of the lungs with an intact trachea (Figure 8g) and any remaining additional tissue was then removed (Figure f).

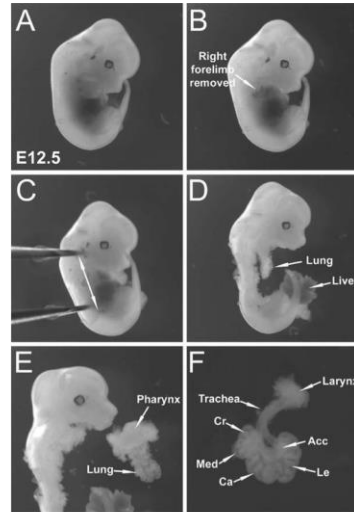


Figure 8. Dissection of E12.5 Mouse Lung. a) E12.5 whole embryo viewed from the side. b) right forelimb has been removed. c) Forceps holding the embryo steady in the dish. Arrow indicates the plan of dissection. d) Embryonic lung lies posterior to the heart and anterior to the spine. Skin and heart have been removed. e) Pharynx removal allows separation of the intact lung from the embryo f) Extraneous pharyngeal tissue and esophagous have been removed. Dissected 12.5 embryonic lung with intact trachea and larynx is shown. Cranial lobe (Cr), Medial lobe (Med), Caudal lobe (Ca), Accessory lobe (Acc), and Left lobe (Le) are identified. Image and caption adapted from del Moral & Warburton, 2010.

The isolated lungs were then transferred using a 200 μ L pipette with a cut pipette tip to a Petri dish containing explant media (Dulbecco's Modified Eagle's Medium/ Ham's F-12 50/50 Mix with L-glutamine supplemented with 5% Fetal Bovine Serum and 1% Penicillin and Streptomycin Solution from VWR).

To culture isolated embryonic lungs, 2 rectangular pieces of polydimethylsiloxane (PDMS) were placed on the floor of a well of a 6 well cell culture plate approximately 5 cm apart (Figure 9). A Whatman nucleopore polycarbonate Track-Etch membrane (8.0 μm) was placed so the edges of the membrane were supported by the PDMS and the center of the membrane was elevated above the floor of the well. (Figure 9b) An isolated lung was placed on the membrane using a 200 μL pipette with a cut tip and positioned using dissection forceps. Lungs were positioned with the right lobes to the left of the left lobe and the accessory lobe visible in the same position as the lung in Figure 4b. Media was removed to allow the lungs to adhere to the membrane via surface tension. New explant media (200 μL) was then added to the well in a semi-circle around the lung culture (Figure 9a). This media was varied depending on the needs of each experiment. 10mL of water was added to an empty well of the 6 well cell culture plate to maintain humidity. The lid was replaced and cell culture plate was placed in a 37°C incubator. Incubation time was varied for the needs of each experiment. A maximum of 2 lungs were cultured per well.

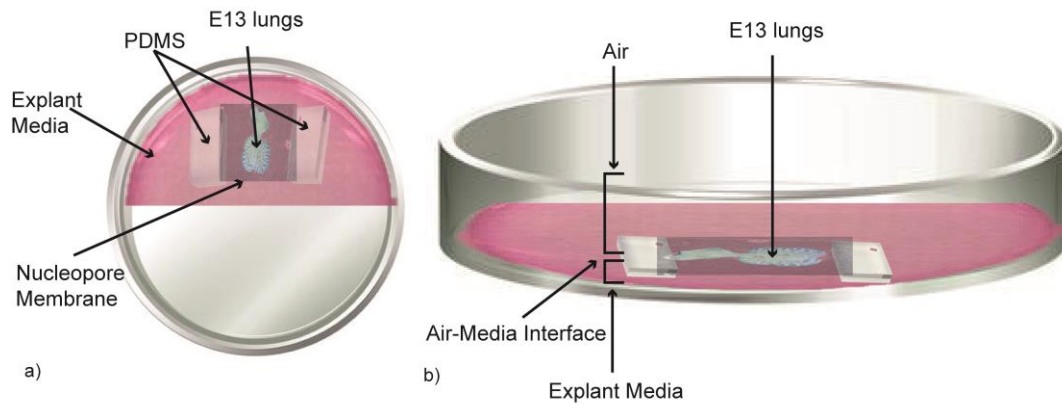


Figure 9. Schematic of E13 Mouse Lung Culture. A pair of embryonic lungs is suspended on a porous nucleopore membrane that is supported off of the floor of the well by two rectangular pieces of polydimethylsiloxane (PDMS). The lung is held to the membrane with surface tension that is applied as the lung sits at the interface of air and media (air-media interface. a) Top view of culture set up b) Side view of culture set up

Lung Structure Analysis (Immunofluorescence)

E13 CD1 lungs were cultured as described above in explant media with varying doses sodium arsenite (0, 0.1, 0.5, 1ng/mL) for 24 hours. At 24hr in culture, lungs were fixed by immersion using 4% paraformaldehyde (PFA) in PBS for 30 minutes at room temperature. Organs were then permeabilized using 0.5% Triton for 2 hours at room temperature and then placed in blocking buffer (1x PBS, 5g BSA, 1g Gelatin, 0.5mL Tween 20x, 5mL 10% NaAzide) over night at 4°C.

To visualize airway epithelium, lungs were labeled using rat anti-E-cadherin monoclonal antibody (Santa Cruz, 1:500) for 2hr at room temperature followed by secondary 488 donkey anti-rat antibody (ImmunoReagents, Inc., 1:500) for 2hr at room temperature. Lungs were also counterstained with DAPI. Wide field images were acquired of the immunostained explants and the widths of the major airways were measured 150 μ m from the carina using Zen 2.6 image processing. Data was analyzed with ANOVA to determine statistical significance of results.

To visualize smooth muscle lungs were immunostained for α -SMA. Lungs were first blocked with Mouse-on-Mouse buffer (Vector Laboratory, 4 μ L/2.5mL PBS) and then labeled using mouse anti- α -SMA monoclonal antibody (Santa Cruz, 1:500) and secondary 550 goat anti-mouse antibody (ImmunoReagents, Inc., 1:500). Lungs were also counterstained with DAPI. High-resolution confocal images were acquired and the thickness of the smooth muscle lining the bronchi was measured (Figure 13).

Western Blot

The amount α -SMA was determined via western blot. 4 E13 CD1 lungs per condition were cultured as above (Figure 9) in control media or media containing 1ng/mL sodium arsenite. Tracheas were removed from the lungs and the remaining lung tissue was lysed in 200 μ L radio immunoprecipitation assay (RIPA) lysis buffer (Alfa Aesar) containing Halt Protease and Phosphatase Inhibitor (Thermo Scientific). Lungs were then sonicated in an ultrasonic ice bath for 5 minutes at 10 second intervals (10 seconds of sonication followed by 10 seconds of rest). Tubes with lysate were then centrifuged at 10,000 rpm for 10 minutes at 4°C. The supernatant was removed and stored in -80° C and the pellet was discarded.

Sample lysate was thawed, and 18 μ L lysate was combined with 6 μ L of 4x SDS sample buffer (final 1x solution: 62.5mM Tris-HCl, 2% SDS, 10% glycerol, 0.002% Bromophenol Blue , 1.5% β -mercaptoethanol). The sample was then boiled at 95°C for 5 min, centrifuged at 10,000 rpm for 30 seconds, and placed on ice before adding to a 12% SDS-PAGE gel for separation.

Samples were separated on gel for approximately 50 minutes running at 150V. Proteins were transferred from the gels to nitrocellulose membranes using a Pierce Power Blot semi-dry transfer system (Thermo Scientific). Transfers were for 7.5 minutes at 24V and 1.3A.

After the proteins were transferred, the membranes were blocked with 5% milk in Tris-buffered saline with Tween-20 (TBST) for 1 hour at room temperature with agitation. The membranes were incubated with a monoclonal rabbit anti α -SMA (Cell Signaling, 1:500) monoclonal antibody at 4°C overnight on with agitation. Blots were then washed with TBST 3 times (5 minutes each wash) and incubated in secondary horseradish peroxidase (HRP)-conjugated goat anti-rabbit (Li-Cor, 1:20,000) antibody for 1hr at room temperature with agitation. Blots were then washed with TBST 3 times (5 minutes each wash). Chemiluminescence was carried out using SuperSingal West Femto Maximum Sensitivity Substrate (ThermoFisher, 1:1) and was captured with a UVP CCD camera in a ChemiDoc-It (UVP) darkroom.

The membranes were then washed with TBST and stripped with stripping buffer (Boston Bioproducts, medium strength). To strip, TBST was replaced with 5mL 1x stripping buffer, and the blot box was incubated for 3 minutes with agitation at room temperature. Stripping buffer was discarded and replaced with fresh 5mL of 1x stripping buffer, and again incubated for 3 min on rocker at room temperature. Stripping buffer was discarded and TBST was added, blot was agitated, and TBST was discarded and replaced with fresh TBST. Blot was washed for 3 minutes at room temp with agitation and stored at room temperature until incubating with primary monoclonal mouse anti-beta-actin (β -actin) antibody (1: 1000, Cell Signaling) overnight at 4°C with agitation followed by washing 3 times with TBST for 5 minutes on rocker at room temperature, incubation with secondary HRP-goat anti-mouse antibody (Li-Cor, 1: 20,000). The remaining procedural steps are the same as listed above from primary through developing except with these different antibodies. The amount of α -SMA was normalized to β -actin and reported as the fold change for α -SMA in lungs cultured in control media compared to lungs cultured in media containing 1ng/mL sodium arsenite. ANOVA was performed to determine statistical significance of results. The results of these two samples were aggregated and displayed (Figure 14).

Contraction Analysis and Kymograph Construction

E13 CD1 (GCaMP lungs used only for calcium signaling assay) lung explants were imaged at 5x on Zeiss AxioObserver inverted microscope with an automated incubation stage while focusing on the epithelium of the lung. Media was replaced at 24 hours in culture to ensure consistent dosing of sodium arsenite and nutrients, and then imaging began. Images were taken at a frequency of 1 Hz for 30-minute periods for a total imaging time of 24 hours. The microscope is only capable of imaging one lung at a time so lungs were imaged in 30 minute rotations. Contractions were observed in the bright field channel and then a custom MatLab script (Appendix b) was used to analyze the number of contractions of the left bronchus during those 30-minute periods. Time lapse CZI videos were converted to AVI format for use with this MatLab code. AVI files were loaded and a line was selected on the first frame of the video. The program then computes the line profile over all of the frames and uses the function VideoReader to save a final tif image where each row represents the selected line at a single frame (Figure 12). This allowed for visualization of an airway overtime at the particular location of interest where the line was placed. Contractions in the airway were visualized and counted. The number of contractions per 30-minute window was recorded and ANOVA was used to determine statistical significance of the contraction frequency among treatment groups.

Calcium/Calmodulin Signaling Analysis

E13 GCaMP lung explants were imaged at 5x on Zeiss AxioObserver inverted microscope with an automated incubation stage at 24 hours in culture after media was replaced with fresh media. Images were taken at 1Hz for 30-minutes. The 5x objective lens was focused on the smooth muscle of the lungs and Calcium/calmodulin binding- induced auto fluorescence was observed in the green fluorescence channel. ImageJ was used to measure mean fluorescence intensity over time and peaks in fluorescence were defined as points in which the mean fluorescence intensity was >50% above baseline fluorescence for a duration of at least 3 seconds. Contractions were also observed on these lungs in the same manner as CD1 lungs as an internal control. ANOVA was used to determine statistical significance of calcium/calmodulin signaling frequency and contraction frequency among treatment groups.

Chapter 3

RESULTS

To study the effect of arsenic, ASM contraction frequency, α -smooth muscle actin (α -AMA) abundance, and calcium signaling characteristics are studied. Embryonic lungs are isolated from pregnant mice and cultured in the presence or absence of arsenic to determine the effect of arsenic exposure to the developing lung. These lungs are then able to be imaged to observed airway smooth muscle contractions to determine if exposure results in a change in the contraction frequency. Immunofluorescence is also performed on these lungs to visualize structural features including the epithelium and smooth muscle (visualized with α -SMA) to compare the airway architecture of treated and untreated lungs as well as the appearance and location of α -SMA. The α -SMA in the lungs is also quantified by western blot to determine the relative abundance in untreated and treated lungs. Finally, lungs are isolated from transgenic mice and imaged to allow the visualization of calcium signaling events. These events are quantified and the relative frequency of calcium signaling events. Together, the results of this study will elucidate the mechanisms underlying lung pathologies associated with arsenic exposure.

Arsenic Affects Embryonic Lung Architecture

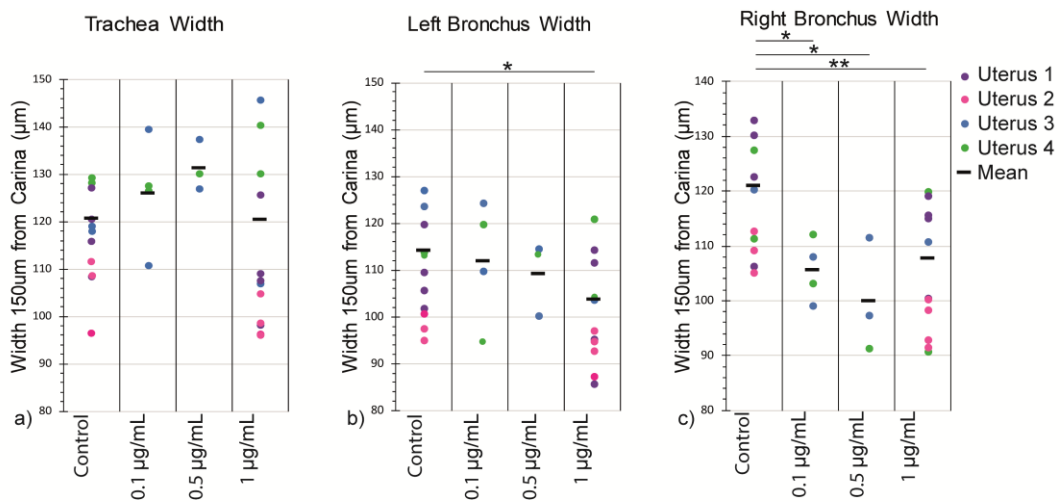


Figure 10. Effects of Arsenic on Embryonic Lung Architecture. Width of a) trachea, b) left bronchus, c) right bronchus of CD1 E13 lungs cultured for 24 hours in varying doses of sodium arsenite (0, 0.1, 0.5, or 1ng/mL) were fixed and immunostained for E-Cadherin. For each lung, the width of airways was measured using zen microscopy software 150um from the carina. Lungs from different uteri represented in different colors and mean is represented with black bar. *p<0.05, ** p<0.01

E13 CD1 lungs were cultured for 24 hours in control or media containing 0, 0.1, 0.5, or 1ng/mL sodium arsenite. (Figure 10) before being fixed, permeabilized, and immunostained for ECAD. There was no significant difference in the width of the trachea among the different treatment groups (Figure 10a). The mean width of the trachea for the control group was 120.9 while the mean for the highest dosed treatment group was 120.6µ. There was a negative correlation between the width of the left bronchus and the dose of sodium arsenite received. As the dose was increased from the control group to the highest dose (1ng/mL), the average width of the trachea significantly decreased from 114.3µm to 103.9µm (p<0.05) (Figure 10b). While the intermediate doses followed the same trend, the average width of the trachea for the intermediate treatment groups (0.1ng/mL: 0.5ng/mL) were not significantly different from the average trachea width of other treatment groups. There was also a significant difference in the average width of the right trachea of the control group compared with

all other intermediate treatment doses. The average width of the right bronchus was 121.2 μm for the control group followed by 105.6 μm ($p<0.05$), 100.1 μm ($p<0.05$), and 107.8 μm ($p<0.01$) for 0.1, 0.5, and 1ng/mL sodium arsenite respectively (Figure 10c). This result suggests that arsenic exposure results in the embryonic lung exhibiting trachea phenotype comparable to untreated lungs, yet narrowed bronchi.

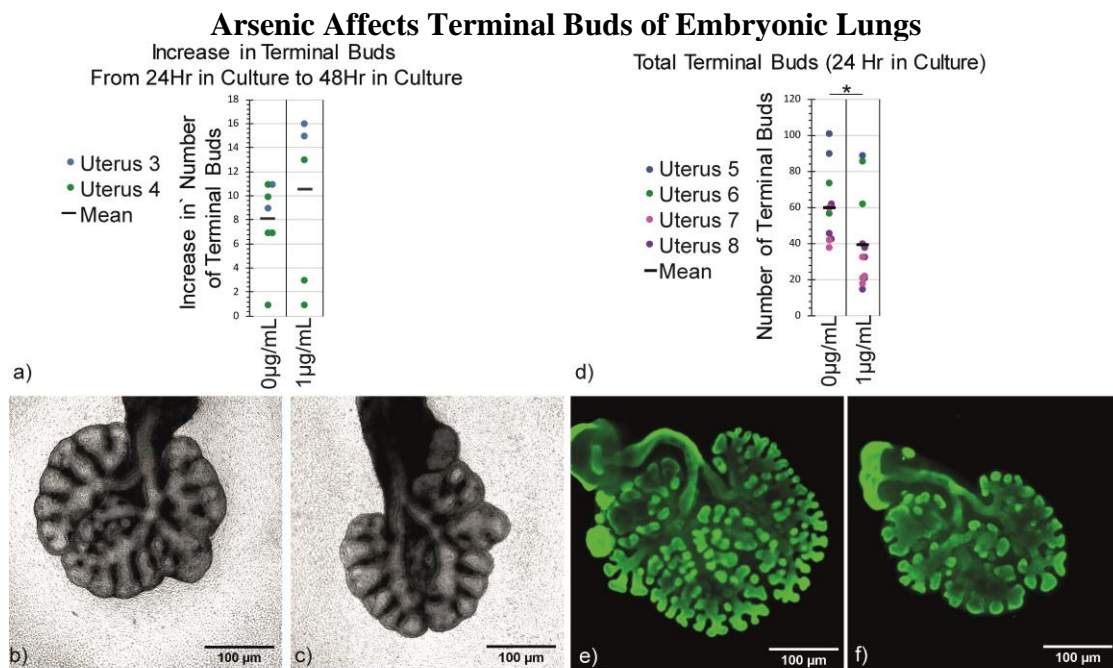


Figure 11. Effects of Arsenic on Terminal Buds of the Embryonic lungs a) E13 CD1 Lungs were cultured in control media or 1ng/mL sodium arsenite and the increase in terminal buds was counted from T24 to T48 hours was counted from T24 and T48 brightfield images. b, c) Representative bright field image of control and treated lungs respectively. d) E13 CD1 lungs were cultured in media control media or 1ng/mL sodium arsenite for 24 hours. Lungs were then fixed and immunostained for E-Cadherin and total number of terminal buds were counted via immunofluorescence microscopy. e,f) Representative immunofluorescence image of untreated and treated lungs respectively. * $p<0.05$

E13 CD1 lungs were cultured in control media or media containing 1ng/mL sodium arsenite and the difference in the number of terminal buds was calculated to determine the increase in 24 hours of culture (11a). There was no significant difference in the increase in terminal buds for control lungs compared to those cultured in 1ng/mL

sodium arsenite. Brightfield imaging analysis presents limitations which may account for being unable to detect a difference in the increase of terminal buds. Terminal buds along the outer aspect of the left lobes, right cranial, and right caudal, lobes are easily visualized and counted, however, the visualization of terminal buds of the right medial and accessory lobes is limited, especially for lobes protruding in the Z direction. For improved visualization of terminal buds, especially those of the accessory lobe, additional lungs were cultured for 24 hours in control or 1ng/mL media and then were fixed, and immunostained for E-cadherin for improved visualization (Figure 11 d,e,f). The terminal buds were counted and totaled for each lung (Figure 11d). Using this protocol, there were significantly more terminal buds after 24 hours of culture in lungs that were cultured in control media compared to with 1ng/mL. Control lungs had on average about 60 (60.36) terminal buds per pair of lungs while treated lungs averaged about 40 (39.83) terminal buds. This result suggest that arsenic exposure results in underdeveloped lungs as evidenced by a reduction in the number of terminal buds present after exposure.

Arsenic Exposure Reduces the Frequency of Airway Smooth Muscle Contraction

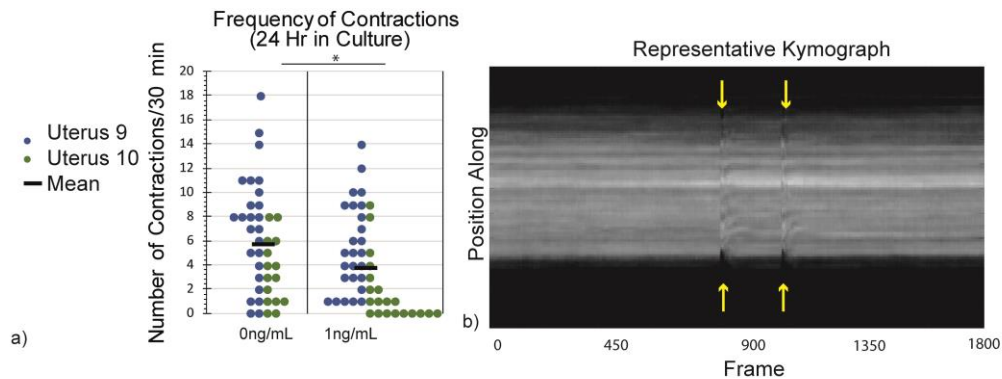


Figure 12. E13 CD1 lungs were cultured in media containing 0 or 1ng/mL sodium arsenite. At 24 hours in culture, brightfield timelapse imaging was performed at rate of 1Hz for 30 minutes for a total of 24 hours (48 hours in culture) to visualize live contractions. Timelapse videos were used to construct kymographs in MatLab to quantify contractions of the left bronchus. a) Representative kymograph constructed in MatLab using 30 minute brightfield timelapse video of an untreated lung (0ng/mL). Two contractions of the airway are indicated by yellow arrows. b) Quantification of the number of contractions observed in 30 minutes for lungs cultured in 0 or 1ug/mL sodium arsenite media. *p<0.05

E13 CD1 lungs were cultured in media control media or 1ng/mL sodium arsenite and contractions of the airway smooth muscle were observed (Figure 12). Time lapse video imaging was used to take live video of each lung for 30 minute segments for an additional 24 hours. Only one lung can be imaged a time so each lung was rotated through 30 minutes of imaging. 8 lungs were typically cultured and imaged per contraction experiment, so the total cycle was 2 hours before the first lung was imaged for a second time. Time lapse video imaging was started 24 hours in culture, continued until 48 hours in culture, and the average frequency of contractions per 30 minute segment was calculated. Contractions were measured in the left bronchus proximal to the first L1 branch point (Figure 4). Time lapse videos were used to construct kymograph using Mat Lab allowing the contractions of the airway to be easily visualized (Figure 12b). On the average 30 minute segment, control lungs contracted 6.26 times while treated lungs exhibited an average of 3.9 contractions. This suggests

that arsenic exposure reduces the frequency of airway smooth muscle contraction which could be a contributor to the underdevelopment of exposed lungs.

Smooth Muscle Quantification Studies



Figure 13. Effect of Arsenic on Airway Smooth Muscle Thickness Along the Inner Bronchi of the Embryonic Lung. E13 CD1 lungs were cultured in control media or 1 ng/mL sodium arsenite for 24 hours. b) Lungs were then fixed and immunostained for E-Cadherin (purple) and α -smooth muscle actin (α -SMA)(red). The width of α -SMA along inner aspects of bronchi was measured 150um from carina (white solid lines) a) Width of α -SMA along bronchi

E13 CD1 lungs were cultured for 24 hours in control media or media containing 1ng/mL sodium arsenite then fixed and immunostained for α -SMA and ECAD and imaged using confocal microscopy. There was no significant difference in the thickness of airway smooth muscle lining the inner aspects of the bronchi. (defined as the area of the lung with positive fluorescence for a-SMA) (Figure 13a). Of the two lungs that were analyzed, the average width of α -SMA for control lungs was 47.5 μ m and for treated the average was 41.5 μ m. There was also no difference in average width of α -SMA along the right bronchi. The average for untreated was 45.1 μ m while the average for treated was 45.75 μ m.

Western Blot Quantification of α -Smooth Muscle Actin

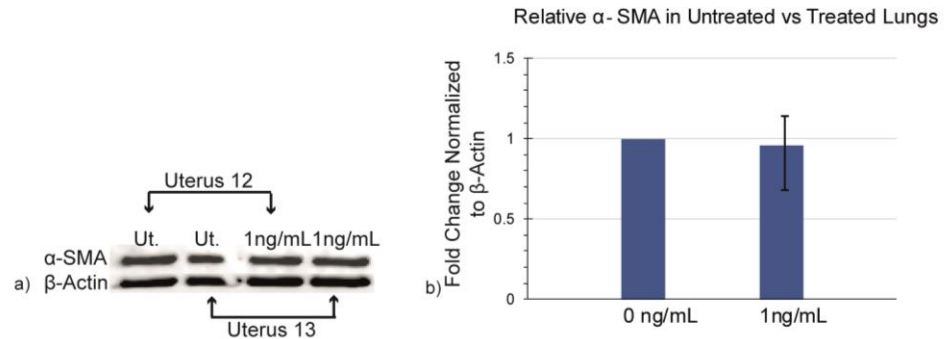


Figure 14. Effect of Arsenic on α -SMA abundance in the Embryonic Lung. Western blot quantification of α -SMA. E13 CD1 lungs were cultured control media or 1 ng/mL sodium arsenite. At 24hrs of culture, 4 lungs were pooled for each condition and whole organ lysate was collected. a) Western blot was performed to quantify amount of α -SMA and β -actin. This was repeated with a second uterus in which 4 lungs were also pooled for each condition. b) Western blot quantification of α -SMA normalized to β -actin

Western blot was used to quantify the amount of α -SMA normalized to beta-actin (β -actin) in E13 CD1 lungs that were cultured in control media or 1ng/mL sodium arsenite (Figure 14a). Each of the two analyzed samples was comprised of 4 lungs per condition. 4 lungs per condition were pooled and whole lysate was collected for analysis via western. There was no significant difference in the amount of α -SMA present in either of the two samples that was analyzed. There was on average a 0.95-fold change in the amount of α -SMA in treated lungs compared to untreated. This result shows that the relative abundance of α -SMA in treated lungs is not significantly different from untreated lungs.

Arsenic Affects Calcium/ Calmodulin Signaling in Embryonic Lungs

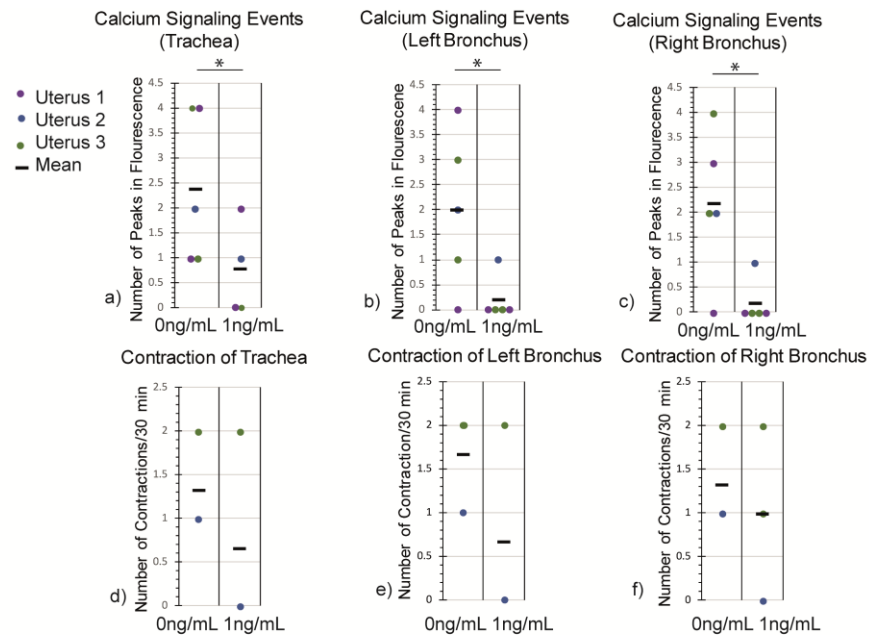


Figure 15: Arsenics affect on calcium signaling in the embryonic lung. E13 GcaMP lungs were cultured in media control or 1ng/mL sodium arsenite. Fluorescence occurs when intracellular calcium binds to calmodulin. a,b,c) At 24hr in culture, timelapse videos were acquired in the green fluorescence channel for a period of 30 minutes. Mean fluorescence intensity over time for each location was measured in the trachea, left bronchus, and right bronchus with ImageJ and peaks were identified as peaks in fluorescence >50% above baseline fluorescence lasting longer than 3 seconds. d,e,f) After 24 hours in culture, contractions were analyzed via brightfield timelapse imaging. in the trachea, left bronchus, and right bronchus. *p<0.05

E13 transgenic GCaMP lungs were cultured in control media or media or 1ng/mL sodium arsenite and live video microscopy was performed to visualize peaks in fluorescence that occur when calcium binds to calmodulin. Videos were acquired in the green fluorescence channel at a rate of 1Hz for 30 minutes. One lung at a time was imaged for 30 minutes prior to imaging the next lung. There were significantly more frequent peaks in fluorescence in lungs that were cultured in 1ng/mL sodium arsenite in the various locations in the lung that were analyzed (Figure 15). Robust calcium waves often, but not always propagated from the trachea through both bronchi in

proximal to distal direction. On occasion signaling events will propagate from the trachea down one bronchus, or initiating and propagating through only one bronchus. Separate areas of the lung were analyzed to account for this. There is no significant difference in calcium signaling occurring in trachea. Control lungs exhibit an average of 2.4 peaks in fluorescence while treated exhibit 0.8 ($P < 0.07$). There are however, significantly more calcium signaling event in control lungs compared treated in both bronchi. In the left bronchus, control lungs had an average of 2 signaling events while treated lungs had an average of just 0.2 ($p < 0.05$). On average, control lungs also exhibited more signaling events in the right bronchus. An average of 2.2 peaks were observed in control lungs compared to 0.2 in untreated. As an internal control, the same lungs were also observed for frequency of contractions. The frequency of fluorescent peaks and the frequency of contractions follow the same trend. There are more fluorescent peaks and contractions observed with control lungs.

Chapter 4

DISCUSSION

Arsenic Exposure Increases the Risk of Respiratory Complications Associated with Preterm Labor

There are an estimated 15 million infants born preterm globally (Quinn et al., 2016) and pregnant mothers living in areas where exposure to arsenic is prevalent have an increased risk of preterm labor as well as miscarriage, stillbirth, and low birthweight (Milton et al., 2017). There are a myriad of health concerns associated with preterm births. Chronic respiratory diseases are a common complication of preterm birth, particularly among very immature infants (Kwinta & Pietrzyk, 2010). Very premature infants are at risk of developing bronchopulmonary dysplasia (BPD) which is a chronic respiratory disease associate with high mortality and co-morbidities (Kwinta & Pietrzyk, 2010). In addition to respiratory complications, a myriad of additional health concerns are associated with preterm births (Kwinta & Pietrzyk, 2010). In addition to the morbidities associated with preterm birth, arsenic increases the risk, directly, for respiratory pathologies including asthma, COPD, and respiratory failure. (Bloom et al., 2014).

This research shows that lungs exposed to arsenic during early stages of development exhibit complex abnormal, underdeveloped phenotypes. The abnormal phenotypes observed in embryonic lungs exposed to arsenic are consistent with observed respiratory abnormalities in human individuals that have been exposed. Specifically, this research has shown that when exposed to arsenic, embryonic lungs have an altered

morphology compared to untreated lungs (Figure 10, 11). Results have shown that arsenic exposure results in underdevelopment of the lung as evidenced by a significant reduction in the width of the right and left bronchi with exposure and a significant reduction in the number of terminal buds compared to untreated lungs.

Arsenic is further causing problems on lungs that are already underdeveloped in preterm infants, resulting in poorer birth outcomes (Bloom et al., 2014).

Underdeveloped lungs are the predecessor to infant lung pathologies and the findings of this research are consistent with the observation that exposure to arsenic results in respiratory diseases. Retarded lung growth is known in some cases to be embryonically lethal (Warburton et al., 2010) and this may be the mechanism through which arsenic is linked to poorer outcomes in preterm infants. This research suggests that poor birth outcomes related to arsenic exposure are due in part to underdeveloped lungs as evidenced by results regarding reduced growth/ development of lungs. The abnormal phenotypes observed in embryonic lungs exposed to arsenic are consistent with observed respiratory abnormalities in human individuals that have been exposed.

Arsenic Reduces the Number of Alveoli Precursors in the Lung, Increasing the Risk for Respiratory Pathologies

Evidence suggests that arsenic in drinking water causes non-malignant lung disease, but nearly all related data concerns exposed adults. While little is understood about how in utero exposure to arsenic affects exposed individuals later in life, a study was completed in Chile to investigate in utero arsenic exposure and long-term lung

function that showed increased lung cancer, bronchiectasis, and other chronic obstructive pulmonary disease mortality several decades after high in utero arsenic exposure (Dauphiné et al. 2011). Adults who had high in-utero exposure also had reduced lung function characterized by a reduction in forced expiratory volume (FEV) and forced vital capacity (FVC) measurements (Dauphiné et al. 2011). These measurements are used to categorize severity of obstructive lung diseases such as asthma and COPD and can be used for the assessment of bronchodilator effectiveness (David and Edwards 2020). Children born preterm are at increased risk for recurrent wheezing and asthma (He et al. 2015). Preterm births are also associated with COPD and lower function later in life (Sonnenschein-van der Voort et al. 2014) as well as BPD (Moss 2006). Lungs of infants that have died BPD exhibit fewer, larger alveoli than normal and exhibit abnormal pulmonary vascular development (Moss 2006).

During the canalicular stage of development (E16.5-E17.5), the terminal lung buds become narrower and then during the “saccular” stage (E18.5 to post natal day 5) they develop numerous small sacs that are the precursors to alveoli (Morrisey & Hogan, 2010). Preterm infants exhibit fewer alveoli which is similar to the findings of this research (Figure 11).

Underdevelopment of E13 embryonic lungs exposed to arsenic was characterized by the narrowing of the major airways and a reduction in the number of terminal buds (Figure 11). The results of this research suggest that arsenic exposure results in a

reduced number of alveolar precursor and thus a suggested decrease in number of alveoli, the tiny sacs of the lungs which allow for rapid gas exchange. (Butler & Tsuda, 2011). This suggests that the risk of developing preterm related diseases are increased in those infants that have been exposed to arsenic. To further explore the mechanism that resulted in under development of lungs exposed to arsenic, airway smooth muscles were studied.

The Reduction in the Frequency of Airway Smooth Muscle Contractions Correlates with Underdevelopment of Arsenic-Exposed Lungs

The role of airway smooth muscle has traditionally been controversial (Paré & Mitzner, 2012) but is recognized to influence the rate of developmental maturation of the lung (Nelson et al., 2017) although it is typically studied in the context of diseases such as asthma and COPD. Branching events in the lung are preceded by long-duration waves of airway smooth muscle contraction (Nelson et al., 2017). Several clinical conditions result in fetal pulmonary hypoplasia, an underbranched lung, which is a major cause of respiratory insufficiency and mortality in newborns ([Jobe and Ikegami, 2000](#); [Smith et al., 2005](#)). Pulmonary hypoplasia often co-presents with mechanical defects in the thoracic cavity, suggesting that abnormal airway branching can result from altered physical loads on the lung, even in the absence of an obvious genetic defect ([Smith et al., 2005](#)).

Embryonic lungs exposed to arsenic exhibited reduced frequency of airway smooth muscle contractions (Figure 12). The reduction in airway smooth muscle contractions is accompanied the underdevelopment of lungs which could be the underlying process behind under development of lungs when exposed to arsenic, poor birth outcomes, and later in life respiratory dysfunction

This data suggests that targeting contractions by increasing them could potentially rescue the developmental defect fetuses that have been exposed to arsenic. Others have suggested a similar target (Nelson et al., 2017). These contraction defects could be due to differences in the amount of smooth muscle present in the lung, which was next tested.

Quantification of ASM by α -Smooth Muscle Actin Immunofluorescence is Limited and is Improved with Western Blot

Airway smooth muscle wraps around the circumference of the airways during development and persists into adulthood (Goodwin et al., 2019). Alpha-smooth muscle actin (α -SMA) is an abundant protein in airway smooth muscle cells that makes it a logical protein for immunostaining to identify airway smooth muscle cells (Wong et al. 1998). Aside from being a good marker, it has a critical role in ASM contractions (Figure 6). Despite α -SMA being a predominant cellular protein in smooth muscle cells, it was an unreliable method for identifying ASM. This is due to an artifact of the immunostain that likely occurred due to the poor ability of antibodies to penetrate cartilage (Crombie et al., 2005) (DiDomenico et al., 2015). Cartilage, in addition to

airway smooth muscle encircles the airways during development with significant localization to the outer aspects of the bronchi (Hines et al., 2013). When imaging whole embryonic lungs that were immunostained for α -SMA, the immunostain failed to show fluorescence in areas where there is known to α -SMA. The presence of cartilage around outer aspects of the bronchi may contribute to the area's lack of positive immunofluorescence. This finding will prevent laborious and expensive attempts at characterizing ASM by immunostaining for airway α -SMA as it showed an unreliable result. Since immunostaining proved to be an unreliable method for quantifying α -SMA western blotting was used as an alternative method.

After normalizing to beta-actin (β -actin) there was no difference in the amount of α -SMA in lungs that were exposed to arsenic (Figure 14). Since the amount of α -SMA was the same yet there was a decrease in frequency of contractions when exposed to arsenic, the regulation the calcium/calmodulin pathway was studied. This regulatory pathway in particular was studied because arsenic interacts with this pathway in vascular smooth muscle (Figure 2).

Defective Calcium-Influx is the Underlying Mechanism of Arsenic-Exposed Lung Underdevelopment

The amount of contraction is a graded, dose-dependent response to calcium (An et al., 2007). As a result, low concentrations of intracellular calcium result in small low contractions while high doses of calcium result in high amounts of contractions (An et al., 2007). Calcium binding to calmodulin precedes airway smooth muscle contraction (Jude et al., 2008). Higher levels of intracellular calcium are needed for contraction

and lower levels of intracellular calcium allow for relaxation (Jude et al., 2008). When intracellular calcium binds to calmodulin, it activates MLCK which in turn phosphorylates the myosin head allowing it to form cross bridges with actin to shorten muscle fibers and cause contractions (Lavoie et al., 2009). Unlike in skeletal muscle, there are various ways to increase the amount of intracellular calcium in airway smooth muscles (Figure 7) (Lavoie et al., 2009). When calcium stores in the sarcoplasmic reticulum (SR) of smooth muscle cells are depleted, calmodulin exists in the cytosol in an inactive state (Shen et al., 2002). When intracellular calcium levels increase however, calcium binds calmodulin which allows calmodulin to activate myosin light chain kinase (MLCK). This varies compared to skeletal muscle in which myosin is always capable of being active and is waiting for the active site of actin to be revealed (Lavoie et al., 2009). In smooth muscle, the binding site of actin is always available but myosin is not active until it has a phosphate group is added to it by MLCK (Lavoie et al., 2009). While calcium ATP-ases restore extracellular calcium and SR calcium stores (Figure 7), increases in intracellular calcium occur when calcium is released into the cytosol from the SR or enters the cell from the extracellular environment through ion channels that are gated in various ways (An et al., 2007). Fast, robust influxes of calcium through membrane ion channels are response to various stimuli including stretch (specifically in cardiac muscle) and depletion of calcium stores from the SR (An et al., 2007). The large, robust calcium/calmodulin events characterized in this research (Figure 15) is characteristic of calcium repletion through calcium channels on the cell membrane.

It was observed that in addition to a reduction in the frequency of contractions (Figure 12), lungs exposed to arsenic have less frequent calcium influxes (Figure 15). Due to the differences in calcium influxes and the knowledge that these events are coupled to contractions (An et al., 2007), this data suggests that the underlying mechanism to arsenic exposed lungs being underdeveloped is this defect of calcium influx.

Chapter 5

CONCLUSION AND FUTURE WORK

Conclusion

Arsenic exposure continues to be a major public health issue affecting millions of people world-wide (Hasan et al., 2019) that arises from its implications to human health including malignancies, cardiovascular disease, respiratory disease, and other pathologies affecting nearly every organ system in the human body (Ratnaike, 2003). Health problems are associated with arsenic exposure whether exposure occurs as an adult, a child, or in utero through trans-placental transport (Ratnaike, 2003, Gerber et al., 1982). Toxicology research regarding arsenic largely regards the consequences of adult exposure to arsenic via contaminated drinking water (Wai et al., 2017) and a gap in knowledge still exists in the underlying mechanisms of arsenic-induced pathologies. (Singh et al., 2011). Specifically, there is little known about how arsenic affects embryonic development, and how it precedes respiratory diseases. A logical target mechanism for studying arsenic-induced respiratory pathologies that develop in response to in utero exposure is the calcium/calmodulin contractile pathway that modulates vascular and gastrointestinal smooth muscle (Singh et al., 2011). The pathways regulating airway smooth muscles has many of the same regulatory molecules and responses to contractile stimuli (Singh et al., 2011; Jude et al., 2008). This research determined that an underlying mechanism contributing to underdevelopment of arsenic exposed lungs is a defect in the intracellular calcium

influx required to activate the contraction of ASM via calmodulin binding. What we still don't know, is the molecular process impairing the influx of calcium into ASM cells and how to go about rescuing this defect.

Future Directions

Additional studies could be performed to validate the results of this research. It is suggested that the reduction in calcium influx results in reduced ASM contraction frequency leading to underdeveloped arsenic-exposed lungs. To validate, the amount of phosphorylation of MLC should be quantified using western blot for the abundance of total MLC and phosphorylated MLC (pMLC) expecting to see that when exposed to arsenic, there is less phosphorylation of MLC due to the reduction of intracellular calcium influx.

To understand the molecular mechanism that prevents the normal influx of calcium into the cytoplasm of ASM cells, the various ways in which intracellular calcium influxes occur must be considered (Figure 7). Broadly speaking, there are two ways in which the levels of intracellular calcium can be increased. First, by entry of calcium from the extracellular environment and second, by release of calcium from the intracellular stores. (Hill-Eubanks et al., 2011). The results of this research indicated that there was a reduction in calcium influxes from the extracellular environment characterized by the sharp, fast, transient peaks in calcium/calmodulin binding-induced fluorescence observed (Figure 15). Immediate future work considers the molecular mechanisms behind this defect in calcium influx. Influx is mediated by ion channels in the membrane, most prominent of which are the voltage- dependent

calcium channel and non-selective cation channels such as TRP channels (Figure 7) (Hill-Eubanks et al., 2011). Suggested future studies include the pathways that regulate the function or expression levels of these receptors and experimentation may include expression assays of these channels of interest or other proteins in the pathway.

For example, Acetylcholine (ACh) is the endogenous agonist for receptors that activate downstream intracellular calcium influxes (Bergner & Sanderson, 2002). Potentially ACh receptors of interest that are involved in calcium signaling are the M2 and M3 muscarinic cholinergic receptor subtypes (Wei et al., 2014). ACh activates both of these receptors and research has shown that the M2 muscarinic receptor-mediated gating of non-selective cation channels requires a rise in cytosolic calcium mediated by the M3 receptors (Jude et al., 2008). Selectively blocking the M2 subtype of muscarinic receptors attenuated the ACh-induced intracellular calcium transients (Jude et al., 2008). The possibility that arsenic mediates calcium transients by reducing the function or expression of one or both of these receptor subtypes cannot be ruled out. Possible experimentation includes RT-PCR to determine expression levels of receptors of interest. In addition to the voltage-gated ion channels regulated by muscarinic receptors, M2 muscarinic subtype receptors also activate TRP channels via the CD38/cADPR signaling pathway (Fig 7) (Jude et al., 2008), targets of which would all be interesting for future exploration of the mechanism underlying the reduction in calcium influxes presented in this research. The implications of these findings would inform the mechanism underlying other muscular pathologies in addition to arsenic-induced respiratory pathologies of the lung.

Airway smooth muscle develops in early stages of lung development and contributes to airway morphogenesis by pushing fluid through the developing lung thus putting pressure on the epithelial wall and encouraging epithelial branching (Nelson et al., 2017). There is a reduction in ASM contractions when embryonic lungs are exposed to arsenic (Figure 12) offering a potential therapeutic target to treat respiratory pathologies involving the underdevelopment of lungs associated with arsenic exposure and/or preterm births. Increasing the frequency of ASM contractions may rescue the normal phenotype of arsenic-exposed lung and or decrease the risk of associated poor birth outcomes. A possible target treatment is one that increases the frequency of contraction downstream of the calcium influx. Since MLCP works independently of calcium to reduce the phosphorylation of MLC and leading to relaxation, MLCK inhibitors would be a logical jumping off place. In addition, agents that increase the activity of MLCK could also potentially rescue the reduced contraction phenotype of arsenic-exposed lungs.

Aside from respiratory-specific pathologies, this research may also guide future research on environmental toxins. Arsenic is a naturally occurring heavy metals in the environment and understanding the underlying mechanism of how arsenic contributes to pathology may guide future research into the effects of other heavy metals such as cadmium and lead for which there is also a lack in knowledge of how they contribute to pathologies when exposure occurs in utero.

REFERENCES

- Aldinger, Kimberly A. et al. 2009. "Genetic Variation and Population Substructure in Outbred CD-1 Mice: Implications for Genome-Wide Association Studies." *PLoS ONE* 4(3). <https://www.ncbi.nlm.nih.gov/pmc/articles/PMC2649211/> (March 19, 2019).
- Amini, M., Abbaspour, K. C., Berg, M., Winkel, L., Hug, S. J., Hoehn, E., Yang, H., & Johnson, C. A. (2008). Statistical Modeling of Global Geogenic Arsenic Contamination in Groundwater. *Environmental Science & Technology*, 42(10), 3669–3675. <https://doi.org/10.1021/es702859e>
- Ammit, Alaina J., Carol L. Armour, and Judith L. Black. 2000. "Smooth-Muscle Myosin Light-Chain Kinase Content Is Increased in Human Sensitized Airways." *American Journal of Respiratory and Critical Care Medicine* 161(1): 257–63.
- An, S. S., Bai, T. R., Bates, J. H. T., Black, J. L., Brown, R. H., Brusasco, V., Chitano, P., Deng, L., Dowell, M., Eidelman, D. H., Fabry, B., Fairbank, N. J., Ford, L. E., Fredberg, J. J., Gerthoffer, W. T., Gilbert, S. H., Gosens, R., Gunst, S. J., Halayko, A. J., ... Wang, L. (2007). Airway smooth muscle dynamics: A common pathway of airway obstruction in asthma. *The European Respiratory Journal : Official Journal of the European Society for Clinical Respiratory Physiology*, 29(5), 834–860. <https://doi.org/10.1183/09031936.00112606>
- Barnes, Peter J. 1998. "Pharmacology of Airway Smooth Muscle." 158: 10.

- de Lanerolle, P., and R. J. Paul. 1991. "Myosin Phosphorylation/Dephosphorylation and Regulation of Airway Smooth Muscle Contractility." *American Journal of Physiology-Lung Cellular and Molecular Physiology* 261(2): L1–14.
- Bergner, A., & Sanderson, M. J. (2002). Acetylcholine-induced Calcium Signaling and Contraction of Airway Smooth Muscle Cells in Lung Slices. *The Journal of General Physiology*, 119(2), 187–198. <https://doi.org/10.1085/jgp.119.2.187>
- Brennan, S. C., Finney, B. A., Lazarou, M., Rosser, A. E., Scherf, C., Adriaensen, D., Kemp, P. J., & Riccardi, D. (2013). Fetal Calcium Regulates Branching Morphogenesis in the Developing Human and Mouse Lung: Involvement of Voltage-Gated Calcium Channels. *PLoS ONE*, 8(11).
<https://doi.org/10.1371/journal.pone.0080294>
- Canning, B. J. (2006). Reflex regulation of airway smooth muscle tone. *Journal of Applied Physiology*, 101(3), 971–985.
<https://doi.org/10.1152/jappphysiol.00313.2006>
- CD-1® IGS Mouse | Charles River. (n.d.). Retrieved March 31, 2020, from
<https://www.criver.com/products-services/find-model/cd-1r-igs-mouse?region=3611>
- Chou, W.-C., Hawkins, A. L., Barrett, J. F., Griffin, C. A., & Dang, C. V. (2001). Arsenic inhibition of telomerase transcription leads to genetic instability. *Journal of Clinical Investigation*, 108(10), 1541–1547.
- del Moral, Pierre-Marie, and David Warburton. 2010. "Explant Culture of Mouse Embryonic Whole Lung, Isolated Epithelium, or Mesenchyme Under Chemically

Defined Conditions as a System to Evaluate the Molecular Mechanism of Branching Morphogenesis and Cellular Differentiation.” *Methods in molecular biology (Clifton, N.J.)* 633: 71–79.

Dixon, Rose E., and Luis F. Santana. 2013. “A Ca²⁺- and PKC-Driven Regulatory Network in Airway Smooth Muscle.” *The Journal of General Physiology* 141(2): 161–64.

Ghorani, V., Boskabady, M. H., Khazdair, M. R., & Kianmeher, M. (2017). Experimental animal models for COPD: A methodological review. *Tobacco Induced Diseases*, 15. <https://doi.org/10.1186/s12971-017-0130-2>

Goodwin, K., Mao, S., Guyomar, T., Miller, E., Radisky, D. C., Košmrlj, A., & Nelson, C. M. (2019). Smooth muscle differentiation shapes domain branches during mouse lung development. *Development*, 146(22). <https://doi.org/10.1242/dev.181172>

Hasan, Md. K., Shahriar, A., & Jim, K. U. (2019). Water pollution in Bangladesh and its impact on public health. *Heliyon*, 5(8), e02145. <https://doi.org/10.1016/j.heliyon.2019.e02145>

Hajjar, I., Hayek, S. S., Goldstein, F. C., Martin, G., Jones, D. P., & Quyyumi, A. (2018). Oxidative stress predicts cognitive decline with aging in healthy adults: An observational study. *Journal of Neuroinflammation*, 15. <https://doi.org/10.1186/s12974-017-1026-z>

- Hilgendorff, A., Reiss, I., Ehrhardt, H., Eickelberg, O., & Alvira, C. M. (2014). Chronic Lung Disease in the Preterm Infant. Lessons Learned from Animal Models. *American Journal of Respiratory Cell and Molecular Biology*, 50(2), 233–245. <https://doi.org/10.1165/rcmb.2013-0014TR>
- Hill-Eubanks, D. C., Werner, M. E., Heppner, T. J., & Nelson, M. T. (2011). Calcium Signaling in Smooth Muscle. *Cold Spring Harbor Perspectives in Biology*, 3(9). <https://doi.org/10.1101/cshperspect.a004549>
- Hindmarsh, J. T., & Savory, J. (2008). The Death of Napoleon, Cancer or Arsenic? *Clinical Chemistry*, 54(12), 2092–2093. <https://doi.org/10.1373/clinchem.2008.117358>
- Hines, E. A., Jones, M.-K. N., Verheyden, J. M., Harvey, J. F., & Sun, X. (2013). Establishment of smooth muscle and cartilage juxtaposition in the developing mouse upper airways. *Proceedings of the National Academy of Sciences*, 110(48), 19444–19449. <https://doi.org/10.1073/pnas.1313223110>
- Hughes, M. F., Beck, B. D., Chen, Y., Lewis, A. S., & Thomas, D. J. (2011). Arsenic Exposure and Toxicology: A Historical Perspective. *Toxicological Sciences*, 123(2), 305–332. <https://doi.org/10.1093/toxsci/kfr184>
- Hunt, Katherine M., Ritesh K. Srivastava, Craig A. Elmets, and Mohammad Athar. 2014. “The Mechanistic Basis of Arsenicosis: Pathogenesis of Skin Cancer.” *Cancer letters* 354(2): 211–19.

- “In Utero Arsenic Exposure and Epigenome-Wide Associations in Placenta, Umbilical Artery, and Human Umbilical Vein Endothelial Cells.”
<https://www.ncbi.nlm.nih.gov/pmc/articles/PMC4844206/> (May 2, 2019).
- International Agency for Research on Cancer, & Weltgesundheitsorganisation (Eds.). (2012). *IARC monographs on the evaluation of carcinogenic risks to humans, volume 100 C, arsenic, metals, fibres, and dusts: This publication represents the views and expert opinions of an IARC Working Group on the Evaluation of Carcinogenic Risks to Humans, which met in Lyon, 17 - 24 March 2009*. IARC.
- Jude, Joseph A., Mark E. Wylam, Timothy F. Walseth, and Mathur S. Kannan. 2008. “Calcium Signaling in Airway Smooth Muscle.” *Proceedings of the American Thoracic Society* 5(1): 15–22.
- Kosnett, M. J. (2013). The Role of Chelation in the Treatment of Arsenic and Mercury Poisoning. *Journal of Medical Toxicology*, 9(4), 347–354.
<https://doi.org/10.1007/s13181-013-0344-5>
- Kulshrestha, A., Jarouliya, U., Prasad, G., Flora, S. J. S., & Bisen, P. S. (2014). Arsenic-induced abnormalities in glucose metabolism: Biochemical basis and potential therapeutic and nutritional interventions. *World Journal of Translational Medicine*, 3(2), 96–111. <https://doi.org/10.5528/wjtm.v3.i2.96>

- Kwinta, P., & Pietrzyk, J. J. (2010). Preterm birth and respiratory disease in later life. *Expert Review of Respiratory Medicine*, 4(5), 593–604.
<https://doi.org/10.1586/ers.10.59>
- Lauzon, A.-M., & Martin, J. G. (2016). Airway hyperresponsiveness; smooth muscle as the principal actor. *F1000Research*, 5.
<https://doi.org/10.12688/f1000research.7422.1>
- Lee, Moo-Yeol et al. 2005. “Inorganic Arsenite Potentiates Vasoconstriction through Calcium Sensitization in Vascular Smooth Muscle.” *Environmental Health Perspectives* 113(10): 1330–35.
- McBride, M.B. 2013. “Arsenic and Lead Uptake by Vegetable Crops Grown on Historically Contaminated Orchard Soils.” *Applied and environmental soil science* 2013. <https://www.ncbi.nlm.nih.gov/pmc/articles/PMC4776765/> (April 24, 2019).
- Milton, A. H., Hussain, S., Akter, S., Rahman, M., Mouly, T. A., & Mitchell, K. (2017). A Review of the Effects of Chronic Arsenic Exposure on Adverse Pregnancy Outcomes. *International Journal of Environmental Research and Public Health*, 14(6). <https://doi.org/10.3390/ijerph14060556>
- Moore, Kimberly A. et al. 2005. “Control of Basement Membrane Remodeling and Epithelial Branching Morphogenesis in Embryonic Lung by Rho and Cytoskeletal Tension.” *Developmental Dynamics* 232(2): 268–81.

Morrissey, E. E., & Hogan, B. L. M. (2010). Preparing for the First Breath: Genetic and Cellular Mechanisms in Lung Development. *Developmental Cell*, 18(1), 8–23.

<https://doi.org/10.1016/j.devcel.2009.12.010>

“Myosin Light Chain Kinase Is Necessary for Tonic Airway Smooth Muscle Contraction.” <https://www.ncbi.nlm.nih.gov/pmc/articles/PMC2820780/> (June 19, 2019).

Nadel, J. A., & Barnes, P. J. (n.d.). *Autonomic Regulation of the Airways*. 20.

Nakamura, K. T., & McCray, P. B. (2000). Fetal Airway Smooth-Muscle Contractility and Lung Development: A Player in the Band or Just Someone in the Audience? *American Journal of Respiratory Cell and Molecular Biology*, 23(1), 3–6.

<https://doi.org/10.1165/ajrcmb.23.1.f188>

Paré, P. D., & Mitzner, W. (2012). Counterpoint: Alterations in airway smooth muscle phenotype do not cause airway hyperresponsiveness in asthma. *Journal of Applied Physiology*, 113(5), 839–842.

<https://doi.org/10.1152/jappphysiol.00483.2012a>

(PDF) *Lung epithelial stem cells and their niches: Fgf10 takes center stage*. (n.d.).

ResearchGate. Retrieved March 30, 2020, from

https://www.researchgate.net/publication/262813027_Lung_epithelial_stem_cells_and_their_niches_Fgf10_takes_center_stage/figures?lo=1

“PII: S0034-5687(00)00208-5 | Elsevier Enhanced Reader.”

<https://reader.elsevier.com/reader/sd/pii/S0034568700002085?token=D3567D9574DE0EF6A7A3EF8E2BAB99BF24F542B458B02E4E27C8C6B8841234984A6751DCF05783FAC531EA352AFB5E7A> (February 19, 2020).

- Quinn, J.-A., Munoz, F. M., Gonik, B., Frau, L., Cutland, C., Mallett-Moore, T., Kissou, A., Wittke, F., Das, M., Nunes, T., Pye, S., Watson, W., Ramos, A.-M. A., Cordero, J. F., Huang, W.-T., Kochhar, S., & Buttery, J. (2016). Preterm birth: Case definition & guidelines for data collection, analysis, and presentation of immunisation safety data. *Vaccine*, *34*(49), 6047–6056.
<https://doi.org/10.1016/j.vaccine.2016.03.045>
- Rankin, S. A., & Zorn, A. M. (2014). Gene Regulatory Networks governing lung specification. *Journal of Cellular Biochemistry*, *115*(8), 1343–1350.
<https://doi.org/10.1002/jcb.24810>
- Rao, Yi, RunHong Li, and DaQing Zhang. 2013. “A Drug from Poison: How the Therapeutic Effect of Arsenic Trioxide on Acute Promyelocytic Leukemia Was Discovered.” *Science China Life Sciences* 56(6): 495–502.
- Ratnaike, R. (2003). Acute and chronic arsenic toxicity. *Postgraduate Medical Journal*, *79*(933), 391–396. <https://doi.org/10.1136/pmj.79.933.391>
- “Relation between in Utero Arsenic Exposure and Birth Outcomes in a Cohort of Mothers and Their Newborns from New Hampshire.”
<https://www.ncbi.nlm.nih.gov/pmc/articles/PMC4977046/> (May 2, 2019).
- Sheller-Miller, Samantha et al. 2016. “Feto-Maternal Trafficking of Exosomes in Murine Pregnancy Models.” *Frontiers in Pharmacology* 7.
<https://www.frontiersin.org/articles/10.3389/fphar.2016.00432/full> (April 17, 2019).

Shen, Y., Lee, Y.-S., Soelaiman, S., Bergson, P., Lu, D., Chen, A., Beckingham, K., Grabarek, Z., Mrksich, M., & Tang, W.-J. (2002). Physiological calcium concentrations regulate calmodulin binding and catalysis of adenylyl cyclase exotoxins. *The EMBO Journal*, *21*(24), 6721–6732.

<https://doi.org/10.1093/emboj/cdf681>

(*Spontaneous Contractility of Human Fetal Airway Smooth Muscle | American Journal of Respiratory Cell and Molecular Biology*, n.d.)

Spontaneous Contractility of Human Fetal Airway Smooth Muscle | American Journal of Respiratory Cell and Molecular Biology. (n.d.). Retrieved January 8, 2020, from <https://www.atsjournals.org/doi/abs/10.1165/ajrcmb/8.5.573>

Tollet, J., Everett, A. W., & Sparrow, M. P. (2002). Development of Neural Tissue and Airway Smooth Muscle in Fetal Mouse Lung Explants: A Role for Glial-Derived Neurotrophic Factor in Lung Innervation. *American Journal of Respiratory Cell and Molecular Biology*, *26*(4), 420–429.

<https://doi.org/10.1165/ajrcmb.26.4.4713>

van Roy, F., & Berx, G. (2008). The cell-cell adhesion molecule E-cadherin. *Cellular and Molecular Life Sciences*, *65*(23), 3756–3788. <https://doi.org/10.1007/s00018-008-8281-1>

Wei, W., Graeff, R., & Yue, J. (2014). Roles and mechanisms of the CD38/cyclic adenosine diphosphate ribose/Ca²⁺ signaling pathway. *World Journal of Biological Chemistry*, *5*(1), 58–67. <https://doi.org/10.4331/wjbc.v5.i1.58>

WHO, Bangladesh—*Sustainable Development & Healthy Environment*. (n.d.).

Retrieved January 8, 2020, from

http://www.whoban.org/sust_dev_mental_env.html

Wu, G., Gentile, L., Fuchikami, T., Sutter, J., Psathaki, K., Esteves, T. C., Araújo-Bravo, M. J., Ortmeier, C., Verberk, G., Abe, K., & Schöler, H. R. (2010).

Initiation of trophoctoderm lineage specification in mouse embryos is

independent of Cdx2. *Development (Cambridge, England)*, 137(24), 4159–4169.

<https://doi.org/10.1242/dev.056630>

Appendix A

CUSTOM MATLAB CODE

```
% Line Analyzer - Program to follow line intensity profile over
time
% this program will load an avi file, let the user select a line within the
% first frame and then computes the line profile over the all frames,
% saving it in a final tif image, where each row represents a single frame.
% The program will accept single color and RGB movies.
% The program is based in part on the SSTPget.m program
% It uses the new MATLAB functions VideoReader and read.
% for older versions, it still contains the old aviinfo and aviread lines
% in the comments section.
% Jan Lammerding
% 10/4/2012
clear
oldCD=cd;
Factor=1; % interpolation factor
na=3; % number of lines to use for averaging
%filename='default';
% Pre-processing: Getting Intensity along line from avi
[filename, pathname]=uigetfile('*.avi','Select myocyte avi-file');
if filename
    cd(pathname);
    file=fullfile(pathname,filename);
    %avi=aviread(file,1);
    aviObj = VideoReader(file);
    Nframes=aviObj.NumberOfFrames;
    %infoavi=aviinfo(file);

    %img=avi.cdata;
    img = read(aviObj, 1);
    %clear avi
    figure(1), set(1,'Name','First Frame','NumberTitle','off');
    imagesc(img), axis image, colormap gray
    nLine=0;
    cont=1;
    while cont
        nLine=nLine+1;
        title(['select line ' num2str(nLine) ': left button - start right
button - end']);
        [x,y]=getline(1);
        [x_2,y_2]=getline(1);
        x=round(x(1:2)); y=round(y(1:2));
        x_2=round(x_2(1:2)); y_2=round(y_2(1:2));

        %computes the intersetion of a_b and u_v
        % a b u and v have to be 2d point vectors eg. a = [3 4];
        x1=x(1); % x1=a(1);
        x2=x(2); % x2=b(1);
        x3=x_2(1); % x3=u(1);
        x4=x_2(2); % x4=v(1);
```

```

y1=y(1); % y1=a(2);
y2=y(2); % y2=b(2);
y3=y_2(1); % y3=u(2);
y4=y_2(2); % y4=v(2);
ua = ((x4-x3)*(y1-y3)-(y4-y3)*(x1-x3))/((y4-y3)*(x2-x1)-(x4-x3)*(y2-
y1));
x_comp = x1 + ua*(x2 - x1);
y_comp = y1 + ua*(y2 - y1);
%calculate the intersection relative to the start of the first line
intersection = sqrt((x_comp-x(1))^2+(y_comp-y(1))^2);

hold on;
plot(x_comp,y_comp, 'r.', 'MarkerSize', 30)

title([filename])
l1(nLine)=line(x,y); set(l1(nLine), 'color', 'r')
set(l1(nLine), 'LineWidth', 2)
h1(nLine)=text(x(2),y(2),['L ' num2str(nLine)]); % label line
[th, r]=cart2pol(x(2)-x(1),y(2)-y(1));
xc(:,nLine)=x(:); yc(:,nLine)=y(:);
xc(2,nLine)=xc(1,nLine)+cos(th)*round(r); %rounded end x
yc(2,nLine)=yc(1,nLine)+sin(th)*round(r); %rounded end y
xi0=linspace(xc(1,nLine),xc(2,nLine),round(r)*Factor);
yi0=linspace(yc(1,nLine),yc(2,nLine),round(r)*Factor);

int=-na:na];
xis{nLine}=[]; yis{nLine}=[];
figure(1)
for i=1:(2*na+1)
    xis{nLine}(i,:)=xi0+int(i)*sin(th);
    yis{nLine}(i,:)=yi0-int(i)*cos(th);
    l3(nLine,i)=line(xis{nLine}(i, [1, length(xi0)]),yis{nLine}(i, [1,
length(yi0)])); set(l3(nLine,i), 'color', 'g')
end
if size(img,3) == 3 % in case we have color image, compute average for
each colorplan
    zis=interp2(double(img(:,:,1)), xis{nLine}, yis{nLine}, '*linear');
% red
    zi(:,:,1)=mean(zis); % use average as 1-D signal
    zis=interp2(double(img(:,:,2)), xis{nLine}, yis{nLine}, '*linear');
% green
    zi(:,:,2)=mean(zis); % use average as 1-D signal
    zis=interp2(double(img(:,:,3)), xis{nLine}, yis{nLine}, '*linear');
% blue
    zi(:,:,3)=mean(zis); % use average as 1-D signal
    zi=uint8(zi); %convert back to uint8 format
else % otherwise only use first colorplan
    zis=interp2(double(img(:,:,1)), xis{nLine}, yis{nLine}, '*linear');
    zi=mean(zis); % use average as 1-D signal
end

Xso=[1:length(zi)]/Factor; % co-ordinates on line (pixel)

```

```

figure(2), set(2,'Name','1D-Data','NumberTitle','off');
plot(Xso,zi(:, :,1))
title(['Intensity along line ' num2str(nLine)]);
xlabel('pixel'); ylabel('intensity')
figure(3), set(3,'Name','Line Profile','NumberTitle','off');
image(zi)
title('average profile along the line')

cont = 0;
end

if nLine % in case we have defined at least one line
% capture line information for entire avi-file
% Nframes=infoavi.NumFrames;
LineImg = uint8(zeros(size(zi,2), Nframes, size(zi,3)));
h=waitbar(0,'Retrieving Data ...');
Lintensity=[];
for n=1:Nframes
% read current frame from avi-file
%avi=aviread(file,n);
imgN = double(read(aviObj, n));
for i=1:nLine

if size(img,3) == 3 % in case we have color image, compute
average for each colorplan
%zis=interp2(double(avi.cdata(:, :,1)), xis{nLine},
yis{nLine}, '*linear'); % red
zis=interp2(imgN(:, :,1), xis{nLine}, yis{nLine},
'*linear'); % red
zi(:, :,1)=mean(zis); % use average as 1-D signal
%zis=interp2(double(avi.cdata(:, :,2)), xis{nLine},
yis{nLine}, '*linear'); % green
zis=interp2(imgN(:, :,2), xis{nLine}, yis{nLine},
'*linear'); % green
zi(:, :,2)=mean(zis); % use average as 1-D signal
%zis=interp2(double(avi.cdata(:, :,3)), xis{nLine},
yis{nLine}, '*linear'); % blue
zis=interp2(imgN(:, :,3), xis{nLine}, yis{nLine},
'*linear'); % green
zi(:, :,3)=mean(zis); % use average as 1-D signal
zi=uint8(zi); %convert back to uint8 format
else % otherwise only use first colorplan
%zis=interp2(double(avi.cdata(:, :,1)), xis{nLine},
yis{nLine}, '*linear');
zis=interp2(imgN(:, :,1), xis{nLine}, yis{nLine},
'*linear');
zi=uint8(mean(zis)); % use average as 1-D signal
end
LineImg(:,n,:) = zi;
end
waitbar(n/Nframes,h);
end

```

```

%clear avi
close(h)

%calculation of the two pixel values to store the intersection
value_first_pixel = floor(intersection/255);
value_second_pixel = round(intersection-(value_first_pixel*255));

%write values into image
LineImg(1,1)= value_first_pixel;
LineImg(1,2)= value_second_pixel;

figure(4), set(4,'Name','Line profile over time','NumberTitle','off');
image(LineImg)
ylabel('position along line')
xlabel('frame')
default_name = [filename(1:end-4) '_result.tif'];
[results_filename, results_pathname]=uiputfile(default_name ,
'Designate file to store results in');
if results_filename
    [path, fname, ext]=fileparts(results_filename);
    results_file=fullfile(results_pathname,[fname '.tif']);

    imwrite(LineImg,results_file);
    disp(['File saved as ' fname '.tif'])
end
end
return
for i=1:4 % close windows
    if ishandle(i)
        close(i)
    end
end
end
cd(oldCD)

```

Appendix B

IACUC Permission

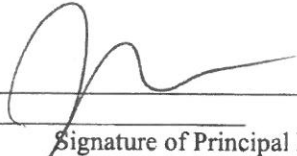
**University of Delaware
Institutional Animal Care and Use Committee
Annual Review**

RECEIVED
MAR 06 2019
IACUC 

Title of Protocol: Mechanical regulation of branching morphogenesis	
AUP Number: 1320-2019-2	← (4 digits only)
Principal Investigator: Jason P. Gleghorn, PhD	
Common Name: House Mouse-multiple strains	
Genus Species: Mus musculus	
Pain Category: (please mark one)	
USDA PAIN CATEGORY: (Note change of categories from previous form)	
Category	Description
<input type="checkbox"/> B	Breeding or holding where NO research is conducted
<input checked="" type="checkbox"/> C	Procedure involving momentary or no pain or distress
<input type="checkbox"/> D	Procedure where pain or distress is alleviated by appropriate means (analgesics tranquilizers, euthanasia etc.)
<input type="checkbox"/> E	Procedure where pain or distress cannot be alleviated, as this would adversely affect the procedures, results or interpretation

Official Use Only	
IACUC Approval Signature:	
Date of Approval:	5.1.19

Principal Investigator Assurance

1. I agree to abide by all applicable federal, state, and local laws and regulations, and UD policies and procedures.
2. I understand that deviations from an approved protocol or violations of applicable policies, guidelines, or laws could result in immediate suspension of the protocol and may be reportable to the Office of Laboratory Animal Welfare (OLAW).
3. I understand that the Attending Veterinarian or his/her designee must be consulted in the planning of any research or procedural changes that may cause more than momentary or slight pain or distress to the animals.
4. I declare that all experiments involving live animals will be performed under my supervision or that of another qualified scientist listed on this AUP. All listed personnel will be trained and certified in the proper humane methods of animal care and use prior to conducting experimentation.
5. I understand that emergency veterinary care will be administered to animals showing evidence of discomfort, ailment, or illness.
6. I declare that the information provided in this application is accurate to the best of my knowledge. If this project is funded by an extramural source, I certify that this application accurately reflects all currently planned procedures involving animals described in the proposal to the funding agency.
7. I assure that any modifications to the protocol will be submitted to the UD-IACUC and I understand that they must be approved by the IACUC prior to initiation of such changes.
8. I understand that the approval of this project is for a maximum of one year from the date of UD-IACUC approval and that I must re-apply to continue the project beyond that period.
9. I understand that any unanticipated adverse events, morbidity, or mortality must be reported to the UD-IACUC immediately.
10. I assure that the experimental design has been developed with consideration of the three Rs: reduction, refinement, and replacement, to reduce animal pain and/or distress and the number of animals used in the laboratory.
11. I assure that the proposed research does not unnecessarily duplicate previous experiments. <i>(Teaching Protocols Exempt)</i>
12. I understand that by signing, I agree to these assurances.
<div style="display: flex; justify-content: space-between; align-items: flex-end;"> <div style="text-align: center;">  <hr style="width: 30%; margin: 0 auto;"/> <p>Signature of Principal Investigator</p> </div> <div style="text-align: center;"> <p>2/15/19</p> <hr style="width: 30%; margin: 0 auto;"/> <p>Date</p> </div> </div>

SIGNATURE(S) OF ALL PERSONS LISTED ON THIS PROTOCOL

I certify that I have read this protocol, accept my responsibility and will perform only the procedures that have been approved by the IACUC.

Name	Signature
1. Jason Gleghorn	
2. Rachel Gilbert	Rachel Gilbert
3. Laurel Schappell	Laurel Schappell
4. Elizabeth Marcin	Elizabeth Marcin
5. Daniel Minahan	
6. Katherine Nelson	Katherine Nelson
7. Mary Athanasopoulos	Mary Athanasopoulos
8. Christine Hillman	Christine Hillman
9. Click here to enter text.	
10. Click here to enter text.	
11. Click here to enter text.	
12. Click here to enter text.	
13. Click here to enter text.	
14. Click here to enter text.	
15. Click here to enter text.	

IACUC approval of animal protocols must be renewed on an annual basis.

1. Previous Approval Date: May 1, 2018

Is Funding Source the same as on original, approved AUP?

Yes **No**

If no, please state Funding Source and Award Number: [Click here to enter text.](#)

2. Record of Animal Use:

Common Name	Genus Species	Total Number Previously Approved	Number Used To Date
1. House mouse	Mus musculus	6584	1920
2. Click here to enter text.	Click here to enter text.	Click here to enter text.	Click here to enter text.
3. Click here to enter text.	Click here to enter text.	Click here to enter text.	Click here to enter text.
4. Click here to enter text.	Click here to enter text.	Click here to enter text.	Click here to enter text.
5. Click here to enter text.	Click here to enter text.	Click here to enter text.	Click here to enter text.

3. Protocol Status: *(Please indicate by check mark the status of project.)*

Request for Protocol Continuance:

A. Active: Project ongoing

B. Currently inactive: Project was initiated but is presently inactive

C. Inactive: Project never initiated but anticipated starting date is:
[Click here to enter text.](#)

Request for Protocol Termination:

D. Inactive: Project never initiated

E. Completed: No further activities with animals will be done.

4. Project Personnel: Have there been any personnel changes since the last IACUC approval?

Yes No

If Yes, fill out the Amendment to Add/Delete Personnel form to “Add” Personnel.

Project Personnel Deletions:

Name	Effective Date
1. Wade Stewart	2/11/19
2. Brain Chambers	2/11/19
3. Click here to enter text.	Click here to enter text.
4. Click here to enter text.	Click here to enter text.
5. Click here to enter text.	Click here to enter text.

5. Progress Report: If the status of this project is 3.A or 3.B, please provide a brief update on the progress made in achieving the aims of the protocol.

Our goal in the animal protocol is to better visualize and quantify the effects of mechanics on the embryonic lung branching morphogenesis. We have been using the CD1 mice to visualize a variety of features of lung development such as airway smooth muscle contractions, and the changes in branching that occur when the lungs are exposed to arsenic. We have also been using the various transgenic mice to uniquely visualize features of the embryonic lungs in real time. We have been able to use the Shh-EGFP/Cre and Shh-CreERT2 mice crossed with Confetti or H2B-mCherry mice to allow us to visualize the lung epithelium during culture. We can then track this epithelium as it grows and deforms by watching it in real time. We have also used the Wt1-EGFP/Cre and Wt1-CreERT2 mice similarly crossed with Confetti or H2B-mCherry mice to do the same but tracking the mesothelial tissue. We are still trying to figure out how to quantify some of the mechanics that are occurring due to airway smooth muscle contractions. These are particularly difficult because they occur on the order of 1 second, and require consistent imaging in 3D. Excitingly, we also started working with the Acta2-GCaMP/mCherry and the Acta2-mCherry mice which allow us to visualize the smooth muscle in real time. These mice have allowed us to visualize the calcium dynamics during a transient smooth muscle contraction that drive many tissue dynamics responsible for growth. We have also been able to visualize what happens when portions of smooth muscle are removed. As hypothesized, the smooth muscle acts as a girdle to guide the branching process, and these experiments have allowed us to visualize this beautifully.

6. Problems or Adverse Effects: If the status of this project is 3.A or 3.B, please describe any unanticipated adverse events, morbidity, or mortality, the cause if known, and how these problems were resolved. If there were none, this should be indicated.

No adverse events, morbidity, or mortality has been incurred by our animals as a result of this protocol during our experiments.